Rochester Institute of Technology

RIT Digital Institutional Repository

5-2-2019

Controllability of Cardiac Alternans

Mark O. Ampofo

moa1953@rit.edu

Controllability of Cardiac Alternans

by

MARK O. AMPOFO

A Thesis Submitted in Partial Fulfillment of the Requirements

for the Degree of Master of Science in Applied and Computational Mathematics

School of Mathematical Sciences, College of Science

Rochester Institute of Technology

Rochester, NY

May 2, 2019

Committee Approval:

_____

Elizabeth M. Cherry, Ph.D.   Date

School of Mathematical Sciences

Thesis Co-Advisor

_____

Laura M. Muñoz, Ph.D.   Date

School of Mathematical Sciences

Thesis Co-Advisor

_____

Nathan D. Cahill, D.Phil.   Date

School of Mathematical Sciences

Committee Member

_____

Matthew J. Hoffman, Ph.D.   Date

School of Mathematical Sciences

Director of Applied and Computational

Mathematics Program

Abstract

An arrhythmia is a disorder in the heart that occurs due to irregular or abnormal heartbeats. There are many types of arrhythmias, some of which are harmless, but some, including ventricular tachycardia and fibrillation, can be life-threatening. Certain arrhythmias are preceded by electrical alternans, which is a state characterized by beat-to-beat alternation in cellular action potential duration. Cardiac alternans may arise from instabilities in either voltage or intracellular calcium cycling. Although a number of techniques have been proposed to suppress alternans, most have focused on appropriately adding a new ionic current or adjusting the timing of pacing stimuli based on the difference between recent action potential durations, rather than affecting intracellular calcium directly. In addition, most of the methods proposed to suppress alternans have been tested using models that do not include calcium-driven alternans. Therefore, it is important to establish a theoretical basis for understanding how control methods may apply when alternans is driven by instabilities in calcium cycling.

In this study, we apply controllability analysis to a discrete map of alternans dynamics in a cardiac cell. In particular, we compare three different controllability measures to determine to what extent different control strategies can suppress alternans. The modal controllability measure was found to be the most informative measure, with effective variables through which to apply control being action potential duration regardless of alternans mechanism along with sarcoplasmic reticulum calcium load in the calcium-driven alternans case. Moreover, we designed and compared three feedback controllers, with the aim of suppressing alternans, based on our controllability results. As expected, full state feedback methods, such as pole placement and the Linear Quadratic Regulator, were more successful in stabilizing unstable alternans modes compared with feedback based on a single variable. We also conducted preliminary work on analyzing controllability of a different model of cardiac alternans described by nonlinear differential equations. Our study provides insight into the feasibility of controlling alternans driven wholly or partially by voltage or intracellular calcium instabilities.

Acknowledgments

First off, I would like to express my special appreciation and thanks to my advisors Dr. Elizabeth Cherry and Dr. Laura Munoz, you have been tremendous mentors for me. I am truly grateful for the time you have invested in my growth as a person and in my career. I hope to make you proud in the future. I would also like to thank Dr. Nathan Cahill for serving as my thesis committee member even at hardship. I thank you for your ingenious comments and suggestions. I also would like to thank Dr. Niels Otani and Alejandro Nieto-Ramos for their valued comments and advice. I am also very thankful to the School of Mathematical Sciences at the Rochester Institute of Technology for opening their doors to me and the wonderful learning environment they provided me with. A special thanks to my family. Words cannot express how grateful I am to my mother for all of the sacrifices that you've made on my behalf. Your prayer for me was what sustained me thus far. Finally, I'd like to thank the National Science Foundation for funding this project through NSF grant CNS-1446312.

Contents

I. INTRODUCTION

Cardiovascular diseases (CVDs) are the leading cause of death worldwide [1]. In 2016, it was estimated that about 841,000 people in the United States died from CVDs [2]. Moreover, between 2014 and 2015, about 14% of total health expenses were allocated to CVDs and stroke, with the medical costs of CVD estimated to more than double from $351 billion to about $749 billion by 2035 [2]. One form of heart disease is arrhythmia, which is a condition defined by irregularities in the heartbeat. Many cardiac-related deaths have been linked to specific types of cardiac arrhythmias, such as ventricular tachycardia (VT) and ventricular fibrillation (VF). In VT, the heart rate in the ventricles (lower chambers of the heart) is fast, whereas in VF, the heart rate in the ventricles not only is fast but also follows a highly irregular or chaotic pattern. As a result of this uncoordinated activity, the ventricles are unable to pump blood, so that VF is fatal within minutes if left untreated. Theoretical and experimental studies [3, 4, 5, 6] have shown that some arrhythmias can be preceded by electrical alternans, which refers to a long and short alternation in the cardiac rhythm that can be observed at the whole-heart level on the electrocardiogram (ECG) as well as in the cellular electrical activations, called action potentials, that trigger contraction. Because alternans can precede the onset of VT and VF, suppressing cardiac alternans may be an approach for preventing some arrhythmias, and methods for control may be useful in doing so.

Previous studies (e.g., [3, 7, 8]) have tested different control algorithms for suppressing alternans. Examples of approaches for eliminating alternans include appropriately adding a new ionic current and adjusting the timing of pacing stimuli based on the difference between recent action potential durations (APDs). Some researchers have applied "chaos control" techniques, such as the methods of Ott, Grebogi, and Yorke [9] or the method of Pyragas [10], to the suppression of alternans, either in theoretical studies or to live tissue [5, 7, 11, 12, 13, 14]. Chaos control methods generally involve adding small perturbations to a system, where the perturbations are chosen in a manner that will stabilize an unstable periodic orbit. When used to suppress alternans, an advantage of certain chaos control methods is that they are relatively straightforward to implement, in the sense that they may only require information about quantities, such as APD, that are easy to measure in a lab setting. A disadvantage of chaos controllers is that the distance over which they can suppress alternans, relative to a stimulating electrode used to apply perturbations to the tissue, is limited [11, 13]. This shortcoming has motivated the investigation of other control techniques, such as state feedback control, as a means of suppressing alternans. "State feedback" typically refers to perturbing a dynamical system by adding a term that is a linear function of

the system state vector. State feedback has been shown to suppress alternans, and in some cases conduction block that occurs when every other stimulus arrives during the refractory period [15], over longer distances relative to a stimulating electrode, compared with chaos control [15, 16, 17]. However, state feedback algorithms often require measurements or estimates of every dynamical variable, not just APD measurements (in the cardiac setting); hence, state feedback is generally more difficult to implement than chaos control.

A smaller number of researchers have applied techniques from modern control theory, such as controllability analysis, to the problem of alternans suppression. The purpose of controllability analysis is to determine whether perturbing one or more of the dynamical equations of a system can feasibly drive the system to a desired state. An advantage of controllability analysis is that it aims to answer questions of control feasibility in a broader sense, based purely on model properties, before a researcher selects, designs, and tests a specific control algorithm, such as state feedback. The controllability of AP dynamics has been investigated, usually with a goal of alternans suppression, in single-cell models [15, 18], an open-ended cable [16, 17, 19], and 2D sheets [20]. There is also a broader class of studies on controllability of reaction-diffusion systems [21, 22], including examinations of reaction-diffusion models that represent cardiac AP dynamics [23, 24, 25]. However, the computational models involved either were not used to differentiate among different sources of alternans or were not capable of representing different mechanisms for alternans.

It has been shown that alternans may arise due to instabilities in voltage [4, 26] or intracellular calcium cycling [27, 28]. Although there is at present no reliable method for identifying the mechanism underlying alternans in a particular scenario, it is possible that alternans arising from different mechanisms may respond differently to different control strategies. Previous studies generally have not considered the role of alternans mechanism on control. This is partly because most of the existing models of cardiac action potentials capable of reproducing alternans were designed to do so only through instabilities in voltage. Recently, a few models have been developed to describe intracellular calcium instabilities as a mechanism for cardiac alternans [28, 29], including some that allow for alternans to be driven by voltage or calcium [30, 31, 32]. Such methods provide an avenue for implementing control methods.

In this thesis, we build on the work of a small number of prior studies, including [15, 16, 18, 19], that used controllability analysis to study control strategies for simulated cells and tissue. Here, we aim to extend these prior studies by comparing several methods for assessing controllability as well as by testing controllability predictions using single-variable feedback and full state feedback

(SF) control methods for voltage- and calcium-driven alternans. Thus, the aims of this thesis are as follows.

- To use controllability analysis to establish a theoretical basis for determining which control strategies are best for suppressing alternans. In particular, we investigate the system variables through which control methods can be applied successfully.

- To determine to what extent the source of the alternans (instabilities in voltage vs. calcium) impacts the best strategy.

- To compare the predictions from controllability analysis for alternans dynamics to outcomes obtained using control methods including single-variable feedback, closed-loop eigenvalue placement, and a linear quadratic regulator (LQR) optimal control technique.

The rest of this thesis is organized as follows. Chapter 2 provides a detailed discussion of the methods, including the models used, controllability analysis as a tool for assessing the effectiveness of control techniques, and feedback control. In Chapter 3, we present the results of applying controllability analysis and feedback control to a discrete-time (difference equation) model as well as preliminary work with a more complicated continuous-time (differential equation) model. In Chapter 4, we present our conclusions and discuss limitations and future work.

II. Methods

This chapter provides a description of two models that describe the nonlinear dynamics of voltage and intracellular calcium cycling in a cardiac cell and that are capable of reproducing cardiac alternans arising from instabilities in voltage and intracellular calcium cycling. In addition, we describe the methods we use to perform a controllability analysis, which can provide a basis for understanding how easily the phenomenon of cardiac alternans reproduced by the two models can be suppressed. Controllability analysis also can provide insights regarding which control strategies (state variables through which control is delivered) may be most effective. Furthermore, we provide a detailed description of the design of control strategies based on the framework established by the controllability analysis. The control strategies we design are based on three feedback techniques: single-variable feedback (SV), pole placement (PP), and the linear quadratic regulator (LQR) state feedback designs.

II.1   Models

In this study we employ two models that describe the dynamics of the membrane potential and intracellular calcium cycling in cardiac cells. Moreover, both models can exhibit alternans arising from mechanisms related to instabilities in voltage and intracellular calcium cycling. The Qu, Shiferaw, and Weiss (QSW) model [31] consists of a system of nonlinear difference equations, while the Shiferaw, Sato, and Karma (SSK) model [32] is a system of nonlinear ordinary differential equations.

II.1.1   The Qu-Shiferaw-Weiss Model

The QSW model is a discrete-time model consisting of four coupled nonlinear difference equations that describe the beat-to-beat evolution of the cardiac action potential duration (APD) and three intracellular calcium concentrations just before applying the next stimulus. The four state variables after the ith stimulus are the APD a_i (ms), the sarcoplasmic reticulum (SR) calcium concentration l_i (μM), the calcium released from the SR r_i (μM), and the total intracellular calcium concentration

b_i (μM). The state variables evolve according to the following equations:

$$a_{i+1} = \frac{f(d_i)}{1 - \gamma c_{i+1}^p} \tag{II.1a}$$

$$r_{i+1} = q(d_i)g(l_i) \tag{II.1b}$$

$$l_{i+1} = l_i - r_{i+1} + \nu u(T)h(c_{i+1}^p) \tag{II.1c}$$

$$b_{i+1} = b_i - \kappa(c_i - c(T)) + \eta(a_{i+1} - a_i) \tag{II.1d}$$

where c_i is the cytoplasmic calcium concentration (μM), d_i is the diastolic interval (ms), c_{i+1}^p is the peak cytoplasmic calcium concentration (μM), and T is the period (ms). The equations also include a series of functions defined in Ref. [31]: $f(d_i)$ is the APD restitution function, $q(d_i)$ defines the restitution properties of SR calcium (Ca) release, $g(l_i)$ describes the dependence of calcium release on the SR load, $u(T)$ describes the period dependence of SR Ca uptake, $h(c_{i+1}^p)$ accounts for the dependence of uptake on peak Ca (note that we have moved the coefficient ν outside this function compared to Ref. [31]), and $c(T)$ is the steady-state cytoplasmic Ca concentration. The quantities c_i, d_i and c_i^p, which represent the intracellular Ca concentration, diastolic interval (DI), and peak intracellular Ca concentration for beat i, are obtained from the state variables as follows.

$$
\begin{aligned}
c_i &= b_i - l_i \\
d_i &= T - a_i \\
c_{i+1}^p &= c_i + r_{i+1}
\end{aligned}
$$

For the default parameter set we used, no alternans occurs for any period. Tab. 1 gives the default values of several key parameters whose values can be adjusted to induce alternans; the remaining parameter values are taken from Ref. [33].

Parameter	Default Value	Units
τ_0	60	ms
ν	0.1	-
Initial Values		
a	197.57	ms
b	117.09	μM
r	2.3762	μM
l	67.791	μM

Table (1)   Key parameter values and initial conditions used for the QSW model.

In this model, voltage instability arises via a steep dependence of APD on the preceding DI (steep

restitution mechanism); fixed points lose stability when the magnitude of the restitution curve slope exceeds one [4]. To promote alternans by steepening restitution (voltage mechanism), the value of τ_0 in $f(d_i)$ was decreased from 60 ms to 30 ms. Calcium-driven alternans arises from instabilities in intracellular calcium cycling. To induce calcium-driven alternans in the QSW model, the value of ν, which scales the strength of calcium uptake into the SR, was increased from 0.1 to 0.4. To produce bifurcation plots showing the periods for which alternans occurs (see Fig. 4), the QSW model was iterated for 1000 cycles at each period, starting from 600 ms and reduced by 20 ms until 80 ms. The final iterated values of a and peak calcium for each period were then plotted vs. period.

II.1.2 The Shiferaw-Sato-Karma Model

The SSK model [32] describes the nonlinear dynamics of voltage and intracellular calcium cycling in a cardiac cell using a system of nonlinear ordinary differential equations. It was developed as a combination of a canine ventricular myocyte model [34] and a model of intracellular calcium cycling [29]. It also provides extra detail compared to the QSW model by including the transmembrane ionic currents and gating variables. The SSK model begins from the Fox et al. canine ventricular model [34], which consists of 11 state variables and can reproduce only voltage-driven alternans. This action potential model then was combined with the Shiferaw et al. calcium cycling model [29] by replacing the original two calcium variable formulations (cytosolic and SR concentrations) with a more detailed calcium cycling submodel, a process resulting in five more state variables. The combined model [32], which we refer to as the Shiferaw-Sato-Karma (SSK) model, can reproduce both voltage- and calcium-driven alternans. It can be written simply as

$$\dot{X} = f_S(X, I_{stim}(t)), \qquad X(t_0) = X_0 \tag{II.2}$$

where $\dot{X}$ is the vector of time derivatives of the state variables and

$$X = [V, m, h, j, X_r, X_s, X_{to}, Y_{to}, d, f, q, c_s, c_i, c_j, c_p^j, I_{rel}]^T$$

is the vector of the 16 state variables: the voltage V (mV), the activation gate m and fast and slow inactivation gates h and j of the fast Na$^+$ current, the rapid delayed rectifier K$^+$ current activation gate X_r, the slow delayed rectifier K$^+$ current activation gate X_s, the transient outward K$^+$ current activation and inactivation gates X_{to} and Y_{to}, the L-type Ca^{2+} channel current activation gate d and voltage- and calcium-dependent inactivation gates f and q, the cytosolic calcium concentration $c_i(\mu M)$, the submembrane space calcium concentration $c_s(\mu M)$, the SR calcium concentration

c_j (μM), the average junctional SR calcium concentration of compartments not being drained c_j'(μM), and the SR calcium release flux I_{rel}($\mu M/s$); I_{stim} is an external stimulus. All variables listed without units are dimensionless. Table 2 shows the initial values and the units for the SSK model.

To promote alternans, we use the SSK model parameterizations of Groenendaal et al. [35], which can lead to instabilities in voltage, calcium, or both. Voltage instability is induced by increasing τ_f, the time constant associated with the f gate, while calcium instability is promoted by increasing u, the load dependence of calcium release from the SR. Here we use the parameter sets for instability through voltage alone ($u = 5$ and $\tau_f = 60$ ms) and through calcium alone ($u = 22$ and $\tau_f = 20$ ms). The SSK model was numerically integrated using an explicit Euler method together with a Rush-Larsen scheme [36] with a time step of 0.01 ms. The applied current I_{stim} was a square-pulse stimulus current of 1 ms duration and 50 mV/ms amplitude [37].

Initial Conditions		
Parameter	Value	Unit
V	-96.08	mV
m	2.4×10^{-4}	-
h	0.9989	-
j	0.9964	-
X_r	2.286×10^{-7}	-
X_s	2.64×10^{-4}	-
X_{to}	3.675×10^{-5}	-
Y_{to}	1.0	-
d	9.255×10^{-8}	-
f	0.9992	-
q	0.8775	-
c_s	0.1	μ M
c_i	0.1	μ M
c_j	150.0	μ mol/l cytosol
c_p^j	150.0	μ M
I_{rel}	1.0×10^{-5}	μ M/s

Table (2)   Initial values used for the SSK model (from [32]).

II.2 Controllability Analysis

Controllability is a property of a dynamical system that describes how strongly the state variables of a system are influenced by inputs to the system [38]. The aim of our controllability analysis is to help us to understand how well alternans due to voltage and intracellular calcium cycling can be suppressed and through which state variables applied control techniques may work more effectively. In particular, we obtain conditions under which the state trajectory can be driven to a non-alternans state by a control input over a finite time interval. In addition, controllability provides us with a framework for designing control techniques for suppressing both voltage- and calcium-driven alternans. In general, to assess controllability, we do the following for each parameter regime and period considered.

- Compute the fixed point.

- Linearize the system about the fixed point.

- Compute controllability matrices based on the linearized system considering each of the state variables in turn as the channel through which to apply perturbations to implement control.

- Compute the rank and minimum singular value ($\sigma_{\min}$) of each controllability matrix, for each combination of parameter regime, period, and state variable used for control.

- Compute modal controllability measures for each linearized system.

II.2.1 Fixed points

The QSW model equations described in Eqn. II.1 above can also be written as

$$X_{k+1} = f_Q(X_k), \tag{II.3}$$

where X_k is the system state at time step k and X_{k+1} is the next state at time step $k+1$. The fixed points are the system states X^* such that

$$X^* = f_Q(X^*).$$

We compute the fixed points for the QSW model by employing MATLAB's `fsolve` function, which attempts to solve $X^* - f_Q(X^*) = 0$ using a trust-region dogleg method. Examples of fixed points are shown in Fig. 1(a)(b). Note that fixed points exist for all periods considered for the parameter

regimes analyzed in this thesis, but in other parameter regimes fixed points are not guaranteed to exist, especially for regimes with dynamics more complex than alternans. We used an initial guess of $[r, a, b, l]^T = [4, 100, 150, 100]^T$, which converged for both voltage-and calcium-driven alternans parameter sets. Estimated fixed points for different periods are shown in Fig. 1(a)(b).

For the SSK model, we obtain a discrete map model by integrating the model $\dot{X} = f_S(X, I_{stim}(t))$ from time t_a to t_b, yielding $X(t_b) = F_S(X(t_a), I_{stim}[t_a, t_b])$, where $I_{stim}[t_a, t_b]$ is the time history of the stimulus current over the interval $[t_a, t_b]$. While we do not know the explicit form of F_S, it can be evaluated by numerically integrating the SSK ODEs over an appropriate time interval. We let $t_b = t_a + T$, where T is the inter-stimulus interval. We can then search for fixed points $X^* = X(t_a + T) = X(t_a)$ of $X(t_a + T) = F_S(X(t_a), I_{stim}[t_a, t_b])$. This can be simplified to $X^* = F_S(X^*)$, since the $I_{stim}(t)$ function is kept identical from one cycle to the next.

To compute the fixed point of the newly defined map for the SSK model, we employ a Newton-Krylov solver [39], which solves a system of nonlinear equations using the Jacobian-Free Newton-Krylov (JFNK) method. The main advantage of using JFNK over the traditional Newton's method is to avoid the need for generating and inverting the Jacobian matrix. Typically the Jacobian matrix is not analytically attainable and its numerical approximation (e.g., via finite-difference methods) is not easily invertible [40]. Starting with the initial condition shown in Table 2 and a period of 800 ms, we used the Newton-Krylov solver to estimate a fixed point. Next, the period was reduced to 780 ms, and we searched for a new fixed point, using the 800 ms fixed point as the initial condition for the search. By continuing this process we obtained fixed points for periods from 800 ms, in intervals of 20 ms, down to 600 ms, and from 590 to 150 ms in intervals of 10 ms. The values of two of the variables at the fixed points are shown as a function of period in Fig. 1(c)(d).

II.2.2 Linearization of the Models

Given a system $X_{k+1} = f(X_k)$ with a fixed point X^*, where we replace f with f_Q or F_S depending on which model is being analyzed, we can linearize the system by Taylor expanding about X^* to obtain

$$x_{k+1} \approx Ax_k. \tag{II.4}$$

Here, $x_k = X_k - X^*$, and the Jacobian evaluated at the fixed point is the state matrix $A = \frac{\partial f}{\partial X}\big|_{X=X^*} \in \mathbb{R}^{n \times n}$. Although the QSW model is time-discrete, its highly nonlinear nature makes calculation of the Jacobian analytically challenging, so instead we compute a numerical approximation of the Jacobian for each period using finite differences with MATLAB. The Jacobian step size

(a) QSW model: voltage-driven alternans

(b) QSW model: calcium-driven alternans

(c) SSK model: V for voltage-driven alternans

(d) SSK model: C^i calcium-driven alternans
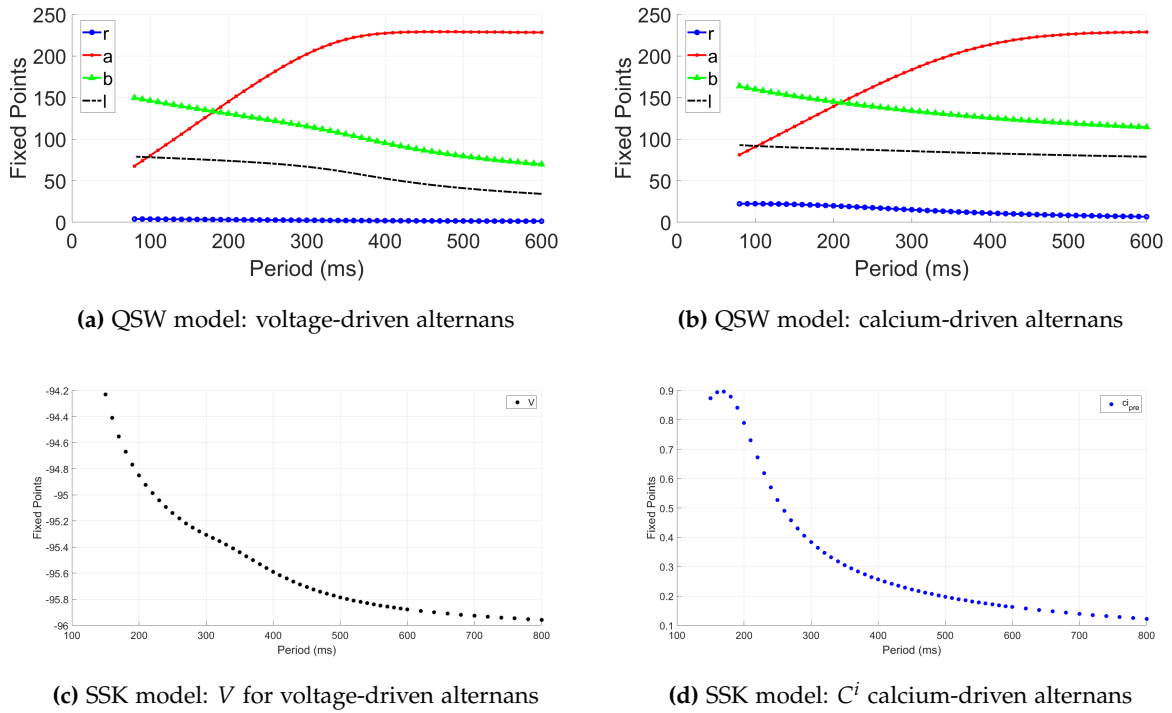
Figure (1) Fixed points as a function of period. (a) QSW model with voltage-driven alternans; all state variables are shown. (b) QSW model with calcium-driven alternans; all state variables are shown. (c) SSK model voltage variable (V) with voltage-driven alternans. (d) SSK model cytosolic calcium concentration variable (C^i) with calcium-driven alternans.

used for the QSW model was 10^{-5}. For the SSK model, we tuned the Jacobian step size in powers of 10 from 10^{-2} to 10^{-12}. We then obtained an optimal step size of 10^{-5}, which minimized the differences in eigenvalues across neighboring step sizes, as will be discussed in more detail later in this thesis. For each model, we computed numerical approximations of the Jacobian for each fixed point using forward and backward differences based on functions provided by C. T. Kelley [39]. A central-differencing step was used to reduce the impact of fixed-point approximation error on the Jacobian.

II.2.3 Controllability

To employ controllability analysis, we begin with a model linearized about a fixed point. The resulting linearized model may be written as

$$x_{k+1} = Ax_k + Bu_k. \tag{II.5}$$

Here, we have augmented Eq. (II.4) with the term Bu_k, where u_k denotes the control input at time step k and $B \in \mathbb{R}^{n \times m}$ is the input matrix, which is a matrix denoting the variables through which control inputs may be applied. Here n is the number of state variables and m is the number of variables through which control is being delivered. Typically, we chose $B = B_j$, where B_j is the jth column of the identity matrix I_n, in order to study the ability to control the system by perturbing one variable at a time.

Both A and B are time-invariant matrices. The system given by II.5 is said to be controllable at k_{initial} if for any arbitrary initial state $x_{k_{\text{initial}}}$ and arbitrary final state x_{final} there exists a finite time index k_{final} and an input sequence $u_{k_{\text{initial}}}, u_{k_{\text{initial}}+1}, \cdots, u_{k_{\text{final}}}$ that will transfer $x_{k_{\text{initial}}}$ to x_{final} at time index k_{final}. If we iterate $x_{k+1} = Ax_k + Bu_k$ through $k_{\text{final}} = n$, we obtain

$$x_n - A^n x_0 = P \begin{bmatrix} u_{n-1} \\ \vdots \\ u_0 \end{bmatrix} \tag{II.6}$$

where $P = \begin{bmatrix} B & AB & A^2B & \cdots & A^{n-1}B \end{bmatrix}$ is referred to as the controllability matrix. The dimension of the controllability matrix is always $n \times nm$. Since the number of control inputs for all our tests is 1, here $m = 1$. Hence for our studies the dimension of P is $n \times n$. If P has full rank, we can solve for the input sequence, given any arbitrary pair of initial and final states x_0 and x_n; this means the system is controllable.

II.2.4   The Rank Test

The rank test is a measure of controllability [41]. The rank of a matrix is defined by the number of linearly independent rows or columns. The system given by Eq. II.5 is controllable if and only if

$$\text{rank}(P) = n.$$

We used MATLAB's function `rank` for computing controllability matrix ranks. If P does not have full rank, we still may be able to control the system if all of the unstable modes of A are controllable. The modal view on controllability will be discussed further later.

II.2.5   Minimum Singular Value Controllability Measure

In cases where the controllability matrix has full rank, the minimum singular value σ_{min} of the controllability matrix may be used as a measure of how close the matrix is to rank deficiency.

For the system to be controllable, the controllability matrix must be nonsingular. $\sigma_{\min} = 0$ means that P does not have full rank, and therefore the system is not controllable, whereas small but nonzero $\sigma_{\min}$ means that the system is weakly controllable. $\sigma_{\min}$ is a function of P, which is in turn a function of the A and B matrices from Eq. II.5. When comparing different control strategies (represented by different B matrices B_i and B_j), we judged one strategy to be better than another if it produced a larger value of $\sigma_{\min}$. MATLAB's `svd` function was used to compute singular values.

II.2.6 Modal Controllability Measure

Another measure of controllability to which we compared singular-value controllability measures is modal controllability. To produce a modal measure of controllability, we start with a linear system, $x_{k+1} = Ax_k + Bu_k$, where A has left and right eigenvectors w_i and v_i and eigenvalues λ_i. Here, $x, B \in \mathbb{R}^n$. Suppose A is diagonalizable. Define $\bar{x} = V^{-1}x$, where the ith column of V is v_i. The ith row of V^{-1} is w_i^*. Applying a similarity transform to the system yields

$$\bar{x}_{k+1} = V^{-1}AV\bar{x}_k + V^{-1}Bu_k$$

$$\begin{bmatrix} \bar{x}_1 \\ \vdots \\ \bar{x}_n \end{bmatrix}_{k+1} = \begin{bmatrix} \lambda_1 & \cdots & 0 \\ \vdots & \ddots & \vdots \\ 0 & \cdots & \lambda_n \end{bmatrix} \begin{bmatrix} \bar{x}_1 \\ \vdots \\ \bar{x}_n \end{bmatrix}_k + \begin{bmatrix} w_1^* \cdot B \\ \vdots \\ w_n^* \cdot B \end{bmatrix} u_k$$

If $w_i^* \cdot B = \|w_i\|\|B\| \cos\theta \neq 0$, then $\bar{x}_i$ can be controlled. An exception occurs when λ_i is repeated and A is diagonalizable, in which case $\bar{x}_i$ cannot be controlled through any single input [41]; in general we will need to perturb as many dynamical equations (through adding more columns to B) as repetitions of λ_j [42].

The modal controllability measure proposed by Hamdan and Nayfeh [43] is based on the cosine of the controllability angles, which indicate how well-aligned the left eigenvectors are with a given B matrix. The cosine of the controllability angle is given by

$$|\cos\theta_{ij}| = \frac{|w_i^* \cdot B_j|}{\|w_i\|\|B_j\|} \tag{II.7}$$

where w_j is the jth left eigenvector of A and θ is the controllability angle. Minimum (more effort) and stronger (less effort) controllability occurs when $|\cos\theta_{ij}|$ takes on values closer to 0 and 1, respectively. If $\cos\theta_{ij} \neq 0$ and λ_i is not repeated, then we say the eigenvalue λ_i of the dynamical system is controllable from input j. Controllability of repeated λ_i is more complicated, as indicated

previously. Negative real-valued λ_i are alternans eigenvalues. "Stable" or "unstable" eigenvalues are used as respective shorthands for eigenvalues that lie within or outside the fixed-point stability boundary $|\lambda| = 1$. If all of the eigenvalues are controllable, then the controllability matrix will be nonsingular [41]. If all of the unstable eigenvalues (if any) are controllable, even if one or more of the stable eigenvalues is not controllable, then the system is said to be stabilizable.

II.3   Single-Variable and State Feedback Control

In this study, we make a distinction between *control strategy* and *control algorithm*. Control strategy refers to which state variable's dynamical equation (i.e., for the QSW model, our choices are the r equation, the a equation, the b equation, or the l equation) we are perturbing to try to suppress alternans. Of course, we could perturb multiple dynamical equations at once, but here we only perturbed one at a time for simplicity. Control algorithm refers to the formula we are using to compute control inputs. An example of a control algorithm is $u_k = \begin{bmatrix} -3 & 0 & 0 & 0 \end{bmatrix} x_k$. For the QSW model, different control strategies are represented by different B_j matrices:

$$B_r = \begin{bmatrix} 1 \\ 0 \\ 0 \\ 0 \end{bmatrix}, \quad B_a = \begin{bmatrix} 0 \\ 1 \\ 0 \\ 0 \end{bmatrix}, \quad B_b = \begin{bmatrix} 0 \\ 0 \\ 1 \\ 0 \end{bmatrix}, \quad B_l = \begin{bmatrix} 0 \\ 0 \\ 0 \\ 1 \end{bmatrix}.$$

Physically we implement B_r by making perturbations to the SR calcium released, B_a by adding a stimulus that changes the duration of the action potential, B_b by adjusting the ionic concentration by injecting calcium, and B_l by making a perturbation to the SR calcium load.

A controllable eigenvalue can be moved through feedback by applying a control algorithm of the form

$$u_k = -Kx_k,$$

where K is a gain matrix with dimension $1 \times n$. This type of control algorithm is known as a state feedback control law and its use makes it possible to rewrite the system $x_{k+1} = Ax_k + B_j u_k$ as a closed-loop state equation of the form

$$x_{k+1} = (A - BK)x_k.$$

Eigenvalues (also known as poles) of the closed-loop system are the eigenvalues of $A - BK$, which are generally different from the λ_i belonging to A. In contrast with "closed-loop systems," the QSW and SSK models are referred to as open-loop systems.

If the controllability matrix is nonsingular, all of the eigenvalues of A may be reassigned to arbitrary locations by adding an appropriate state-feedback term to the dynamical equations. In the weaker case where the system is at least stabilizable, useful control designs are still possible, since any unstable eigenvalues may be reassigned [41]. In this study, we tested three types of controllers: single-variable feedback (SV), pole placement (PP), and a linear quadratic regulator (LQR). In all cases, the goal of the control strategy is to stabilize any unstable modes, including alternans, if it occurs. In other words, feedback control helps us to construct various control designs to suppress alternans.

II.3.1 Single-variable Control

Single-variable feedback control is a method that attempts to stabilize a fixed point by perturbing a system with a term that is based on only one state variable. The feedback control law is given as

$$u_k = -K_{SV}x_k,$$

where the feedback gain K_{SV} is a $1 \times n$ row vector. The key feature of single-variable feedback is that all of the K_{SV} components are zero except for one entry. For the QSW model, this can be rewritten as

$$u_k = -[K_r \quad K_a \quad K_b \quad K_l]x_k.$$

We tested "matched" configurations: if $B = B_r$, then $K_r \neq 0$; if $B = B_a$, then $K_a \neq 0$, etc. The closed-loop state equation for single-variable state-feedback control is then given by the form

$$x_{k+1} = (A - BK_{SV})x_k.$$

II.3.2 Pole Placement

Pole placement (PP) is a state feedback method employed to relocate eigenvalues to desired locations in the unit circle. The method feeds back through all the state variables of the system. Hence, for the QSW model feedback occurs through the four state variables and for the SSK model it is through the 16 state variables. The state feedback control law for PP is given as

$$u_k = -K_{PP}x_k,$$

where the feedback gain K_{PP} is a $m \times n$ matrix. The closed-loop state equation for PP is then given in the form

$$x_{k+1} = (A - BK_{PP})x_k.$$

We used MATLAB's `place` algorithm to compute a gain K_{PP} that places the eigenvalues of $(A - BK_{PP})$ at locations of our choosing.

II.3.3 Linear Quadratic State Feedback Control

The main aim of the Linear Quadratic Regulator (LQR) is to relocate eigenvalues to "optimal" locations in the unit circle by minimizing a quadratic cost function. The idea of the LQR is similar to the other state feedback methods; however, the gain value is selected directly by the user for single-variable state-feedback control and as a function of the desired eigenvalues for pole placement, and in contrast with the LQR gain, the K_{SV} and K_{PP} gains may not be optimal in any sense.

For our discrete system we have

$$
\begin{aligned}
x_{k+1} &= Ax_k + Bu_k, \\
u_k &= -Kx_k, \\
x_{k+1} &= (A - BK)x_k,
\end{aligned}
$$

where K is the feedback gain. The LQR cost function is defined as

$$J(K) = \sum_{k=1}^{\infty} x_k^T Q x_k + u_k^T R u_k,$$

where we choose Q as a positive semidefinite matrix that represents the penalty on the deviation of the state vector from the origin and R as a positive definite matrix that represents the penalty on the magnitude of the control input u [44]. Since $u_k = -Kx_k$, the cost function J is a function of the feedback gain K. The sign-definiteness constraints on Q and R help to ensure the existence of a K that minimizes J. We used MATLAB's `lqr` function to solve for $K = K_{LQR} = \min_K (J(K))$, given the Jacobian A, input matrix B, and penalty matrices Q and R. Our typical choices for penalties were $Q = I_n$ and $R = \alpha_{RQ}\|Q\|$, and we tested various values of $\alpha_{RQ} > 0$, where α_{RQ} is the R-Q ratio. For diagonal Q, allowing Q to be positive semidefinite (but not positive definite) would represent a decision not to penalize one or more state variables, but for our study, we decided to penalize all components of x.

III.   RESULTS

In this chapter we present our main results. In particular, we present our controllability analysis for the QSW model including fixed-point analysis and tests of controllability using the rank, minimum singular value, and modal controllability tests. Furthermore, for comparison with our controllability results we present feedback results for the QSW model using three controllers: SV, PP and LQR. We compare the controllers, including their consistency with controllability predictions, and we quantify the impact of the controllers on the closed-loop eigenvalues, in addition to testing the linearized system response to selected LQR controllers. In addition, we present preliminary work toward controllability analysis for the SSK model, including the results of fixed-point and eigenvalue analysis as well as tuning of the Jacobian step size.

III.1   Fixed Point and Linearization Results for the QSW Model

We successfully found fixed points for the QSW model for both parameter sets we considered and for a broad range of periods. Examples of the results of our fixed-point and linearization analysis are shown in Fig. 2 for the case of voltage-driven alternans. As the period is decreased, the fixed point loses stability when at least one eigenvalue has a magnitude greater than one. Hence, the eigenvalue modulus plot indicates that the fixed points are unstable for periods shorter than 290ms. The unstable eigenvalue is an alternans eigenvalue, as shown via magenta color-coding in the plot for eigenvalues with negative real part. The expected long-run behavior of the model is confirmed in the time-series plots, which show convergence of the APD a and the derived peak calcium concentration c_p after iterating the dynamical equations at a period of 350ms along with alternating (period-2) behavior for a period of 260ms.
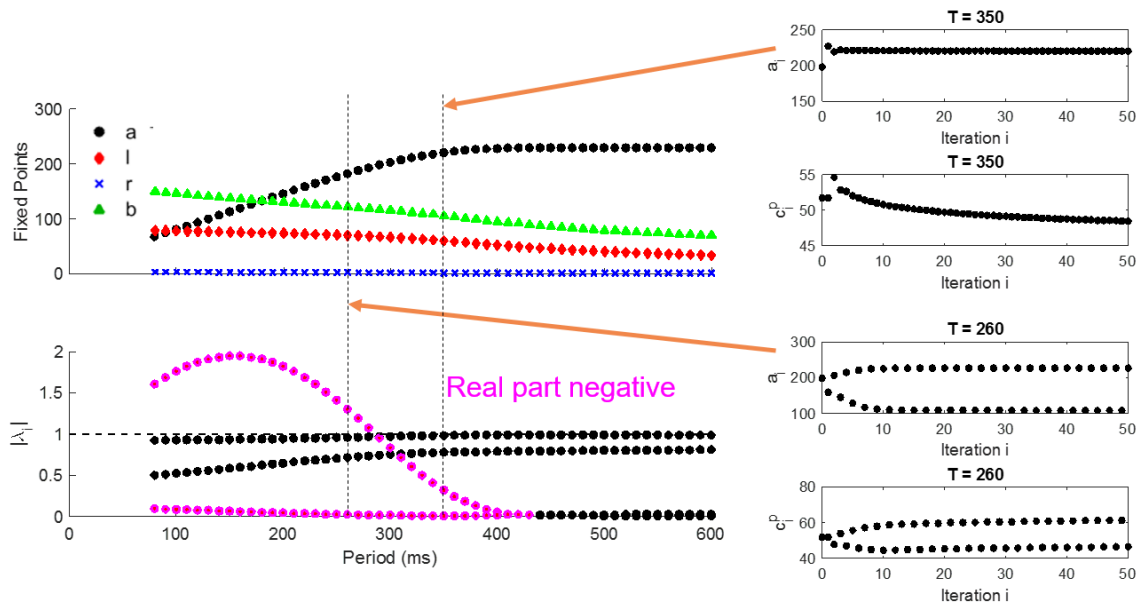
Figure (2) Fixed points and QSW model behavior with voltage-driven alternans. Upper and lower left plots: fixed points and moduli of the eigenvalues as a function of period. The black, red, blue and green curves correspond to the values of a, l, r and b at the fixed point for each period. Alternans arises for periods where at least one eigenvalue has a negative real part (shown in magenta). Right: Examples of a_i and c_i^p vs. iteration index i for periods of 350 and 260 ms.

III.2   Controllability Results for the QSW Model

We computed three different measures of controllability: the rank test, the minimum singular value test, and the modal controllability test. All the results described below are based on the linearized QSW model and the approaches described in the Methods section.

III.2.1   Rank Test

As a first assessment of controllability for the QSW model, we calculated the ranks of the controllability matrices (P) for different control strategies as discussed in the Methods section. When the rank of P is 4, it has full rank, meaning that the system is controllable. Figures 3a and 3b show the ranks obtained for a range of periods for cases of voltage- and calcium-driven alternans, respectively, as control is applied through each of the four state variables r, a, b, and l. Regardless of the alternans mechanism, rank(P) for each period tested is 1 or 4. Specifically, when control is applied through only the SR calcium release r (i.e., $B = B_r$), rank(P) is 1. However, when control is applied through only the APD a, total intracellular calcium concentration b, or the SR calcium load l, rank(P) is 4, indicating that the system is controllable through this variable. Overall, the results from the rank test indicate that the system is controllable through all variables except r for both voltage- and calcium-driven alternans.

(a)   **(b)**
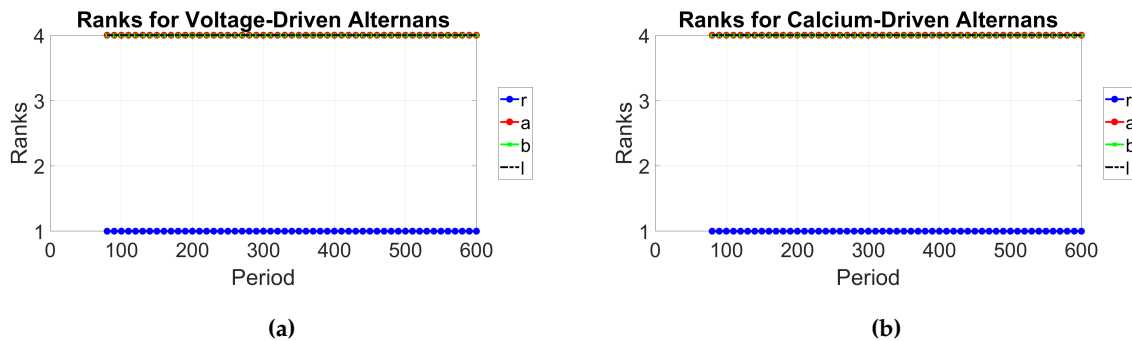
Figure (3)   Ranks of controllability matrices based on different control strategies (B matrices) as a function of period for alternans driven by (a) voltage and (b) calcium instability.

III.2.2   Minimum Singular Value Test

Although we determined that the controllability matrices have full rank for some of the control strategies, the rank test does not indicate the relative magnitude of controllability for each of

these strategies. Hence we consider $\sigma_{\min}(P)$, which is a measure of how close to or far from rank deficiency the matrix P is, as a measure of the magnitude of controllability. Figure 4 shows steady-state a, peak calcium (Ca_i^p), and $\sigma_{\min}(P)$ for periods between 80 and 600 ms for voltage- and calcium-driven alternans. As shown in Fig. 4a, APD and peak calcium bifurcate at a period of about 290 ms for voltage-driven alternans, with a loss in stability of the fixed points for periods below 290 ms (also see Fig. 2). Within the range of periods with alternans, the values of $\sigma_{\min}(P)$ when using B_a are closer to zero and those obtained using B_l are the largest, indicating that control should be easiest when applied through the SR load and most difficult when applied through the APD. Similarly, for calcium-driven alternans, APD and peak calcium bifurcate at a period of about 240 ms (see Fig. 4b), corresponding to a loss in stability of the fixed point. We also observe that within the alternans regime the values of $\sigma_{\min}(P)$ associated with control through the l, b and a variables are farther from zero, indicating that control is more effective when applied through those variables than through r.

(a)   **(b)**
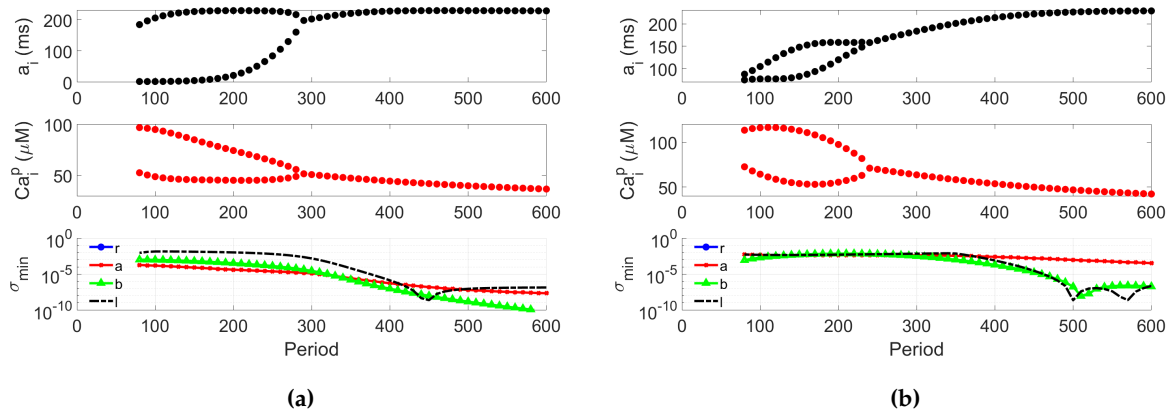
Figure (4)   (a) Voltage-driven alternans: for periods with alternans (indicated by the bifurcated regions in the top two rows of plots), the bottom plot (σ_{min}) shows that control was easiest through the SR load l and most difficult through the APD a. (b) Calcium-driven alternans: for periods with alternans, control was easiest through the SR load l, total Ca^{2+} b, or APD a. In both cases, $\sigma_{min,r} \approx 0$ so it does not appear on a log plot.

III.2.3 Modal Controllability Test

We also applied the modal controllability test to the QSW model. Figures 5 and 6 show the controllability magnitudes ($|\cos\theta_{ij}|$) for all four eigenvalues λ_i, with separate plots for the different control strategies (represented by $B_j = B_r$, B_a, B_b, or B_l), over a range of periods for voltage- and calcium-driven alternans, respectively. Minimum controllability occurs when $|\cos\theta_{ij}| = 0$ (black) and stronger controllability occurs when $|\cos\theta_{ij}| = 1$ (gold). Thus, we will identify the best control strategies as those for which every eigenvalue whose magnitude is greater than one has strong controllability (gold). In the case of voltage-driven alternans, the best control strategy (stronger controllability) for alternans involves delivering control through a, whereas weaker controllability occurs when control is applied through any of the other state variables.
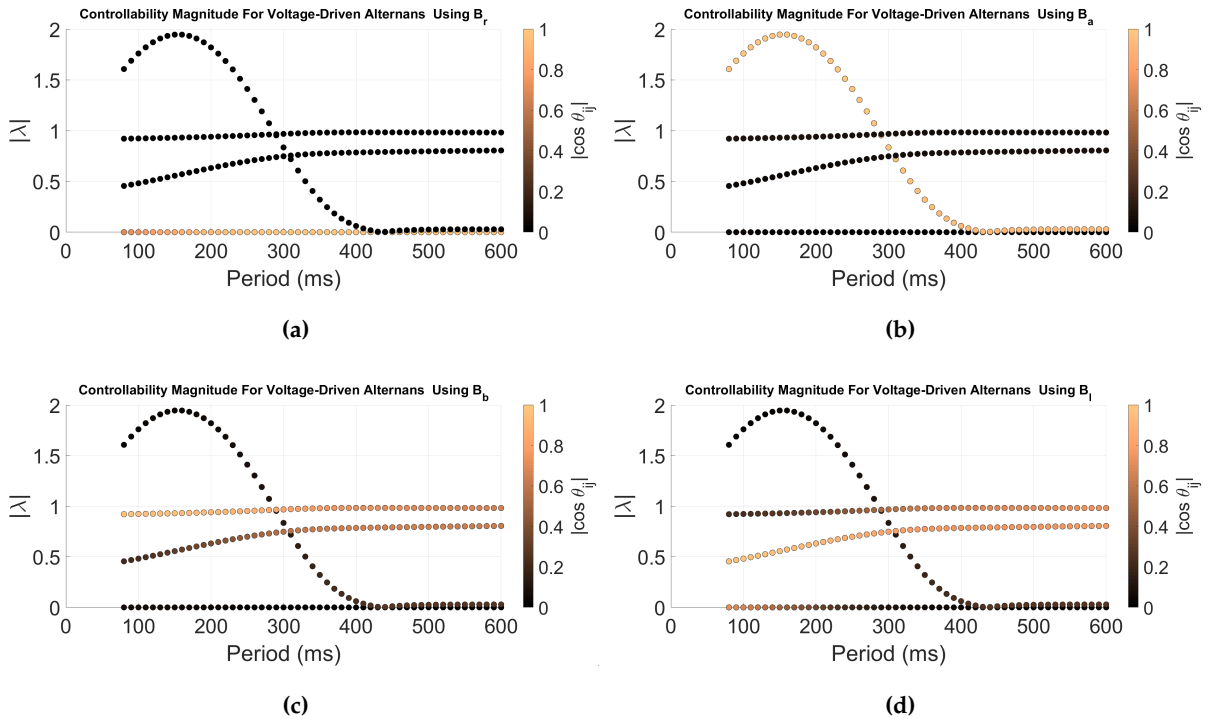
Figure (5) Controllability magnitude as a function of period for voltage-driven alternans using different control strategies: (a) B_r (control through r), (b) B_a (control through a), (c) B_b (control through b), and (d) B_l (control through l).

Similarly, Fig. 6 shows that for calcium-driven alternans, controllability is stronger through a and l and weaker through the other state variables. Thus, our modal controllability results indicate that alternans may be controlled through APD for either alternans mechanism and that SR calcium

load is an additional promising channel for control for calcium-driven alternans.
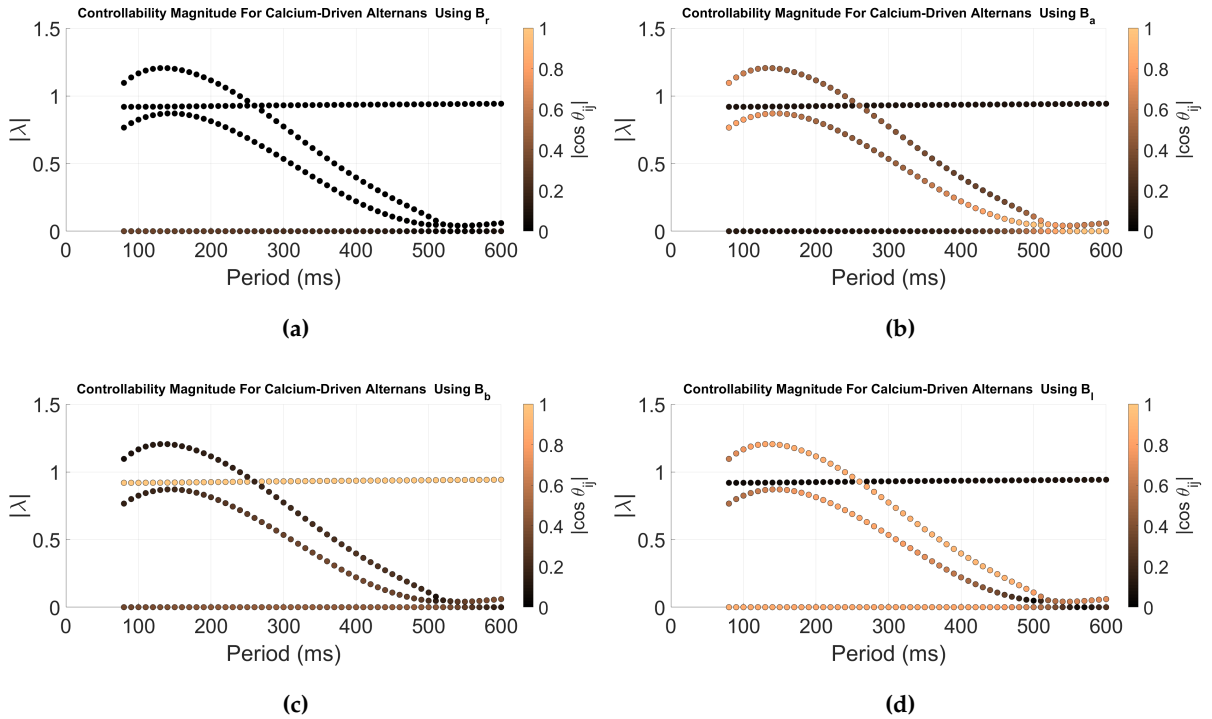
Figure (6) Controllability magnitude as a function of period for calcium-driven alternans using different control strategies: (a) B_r (control through r), (b) B_a (control through a), (c) B_b (control through b), and (d) B_l (control through l).

III.3 State Feedback Results for the QSW Model

Informed by our controllability results for the QSW model, we explored three feedback strategies: single-variable feedback (SV), pole placement (PP), and the linear quadratic regulator (LQR). We compared the maximum closed-loop eigenvalue moduli for the SV and PP approaches and also selected R-Q ratios for the LQR strategy and computed corresponding optimum gains.

III.3.1 Comparing Maximum Eigenvalue Moduli for Single-Variable Feedback and Pole Placement for Voltage- and Calcium-Driven Alternans

We compared the maximum closed-loop eigenvalue moduli for the single-variable and pole placement state-feedback controllers. We focused on applying the controllers through the strategies associated with APD (B_a) and SR calcium load (B_l) for voltage- and calcium-driven alternans,

since these strategies had more favorable modal controllability results. The designs of the SV and the PP controllers and their respective gains can be found in the Methods section.

Voltage-driven Alternans with Control Applied Through the APD (B_a)

To test the SV controllers, we hand-tuned gain values. Values in the range of -100 to 100 were considered. Table 3 shows the "best" gains that we found, in the sense of minimizing the maximum closed-loop eigenvalue modulus, for the range of periods shown in the table with $B = B_a$ in the case of voltage-driven alternans. K_{SV} represents the gain and λ_{SV} represents the closed-loop eigenvalues for SV. As shown in the table, the SV controllers performed well in stabilizing the fixed points, which were open-loop unstable for this range of periods, by decreasing the maximum eigenvalue moduli below one. Also, the gains increased with decreasing period, although it is difficult to conclude anything about the relative difficulty of control across periods, since increasing gains also led to decreasing maximum eigenvalue moduli.

Period (ms)	K_{SV,B_a}	Max ($|\lambda_{SV,B_a}|$)
270	-2.10	0.8759
260	-2.19	0.8633
250	-2.27	0.8538
240	-2.35	0.8411

Period (ms)	Max ($|\lambda_{SV,B_a}|$)	Max ($|\lambda_{PP,B_a}|$)
270	0.8759	0.9593
260	0.8633	0.9563
250	0.8538	0.9533
240	0.8411	0.9505

Table (3)   Best gains for minimizing the closed-loop eigenvalue modulus for voltage-driven alternans using the SV controller with B_a.

Table (4)   Maximum closed-loop eigenvalue moduli for voltage-driven alternans using the SV and PP controllers with B_a.

Table 4 compares the maximum magnitude of the closed-loop eigenvalues for SV and Pole Placement (PP) controllers. λ_{PP} represents closed-loop eigenvalues for the PP controller. The "pole placement" step consisted of specifying the following desired closed-loop eigenvalue locations: $[\frac{\lambda_1}{2} \ \lambda_2 \ \lambda_3 \ \lambda_4]$, where λ_1, λ_2, λ_3, λ_4 are the eigenvalues of A listed in order of decreasing modulus. Our intent in halving the largest eigenvalue was to create PP controllers that would stabilize the fixed points; of course, other designs are possible that would move the eigenvalues farther inside the unit circle. Next, we computed K_{PP} to yield the desired eigenvalue locations. The $\max(\lambda_{PP})$ values in Table 4 thus match the moduli of the second-largest open-loop eigenvalue. Even though we obtained smaller maximum closed-loop eigenvalue moduli for SV compared with PP, based on Table 4 we cannot draw a conclusion about which control strategy performed better, since we have

not attempted to hold the maxiumum eigenvalue modulus (or alternatively, the gain magnitude) fixed across control algorithms.

Voltage-driven Alternans with Control Applied Through the SR Calcium Load (B_l)

When control was applied through the SR calcium load rather than through APD, the best gains we found using SV feedback for periods associated with voltage-driven alternans were unable to stabilize the unstable fixed points (maximum closed eigenvalue modulus was greater than one), even though more effort was being applied by increasing the gains as the period decreased, as shown in Table 5. Moreover, Table 6, which compares the maximum closed-loop SV and PP eigenvalue moduli, shows that the PP controller could always stabilize the unstable fixed points and thus performed better than the SV strategy when control was applied through B_l, in contrast with the B_a case, where it was unclear which control algorithm performed better.

Period (ms)	K_{SV,B_l}	Max ($|\lambda_{SV,B_l}|$)
270	1.86	1.1373
260	1.96	1.2507
250	2.07	1.3669
240	2.14	1.4593

Table (5) Best gains for minimizing the closed-loop eigenvalue modulus for voltage-driven alternans using the SV controller with B_l.

Period (ms)	Max ($|\lambda_{SV,B_l}|$)	Max ($|\lambda_{PP,B_l}|$)
270	1.1373	0.9593
260	1.2507	0.9563
250	1.3669	0.9533
240	1.4593	0.9505

Table (6) Maximum closed-loop eigenvalue moduli for voltage-driven alternans using the SV and PP controllers with B_l.

Calcium-driven Alternans with Control Applied Through the APD (B_a)

Table 7 shows that the best gains for the SV controller using the B_a control strategy were only able to stabilize the unstable fixed points for periods of 200 ms or longer for calcium-driven alternans; the magnitudes of the maximum closed-loop eigenvalues were greater than one for periods shorter than 200 ms. Moreover, Table 8 indicates that the PP controller performed better when compared with the SV controller for control through APD (B_a), since the maximum magnitudes of all closed-loop eigenvalues were less than one.

Period (ms)	$\mathbf{K_{SV,B_a}}$	Max ($|\lambda_{SV,B_a}|$)
220	-1.78	0.9290
210	-1.86	0.9581
200	-1.93	0.9857
190	-2.0	1.0114
180	-2.08	1.0345
170	-2.14	1.0548

Table (7) Best gains for minimizing the closed-loop eigenvalue modulus for calcium-driven alternans using the SV controller with B_a.

Period (ms)	Max ($|\lambda_{SV,B_a}|$)	Max ($|\lambda_{PP,B_a}|$)
220	0.9290	0.9256
210	0.9581	0.9249
200	0.9857	0.9243
190	1.0114	0.9236
180	1.0345	0.9230
170	1.0548	0.9224

Table (8) Maximum closed-loop eigenvalue moduli for calcium-driven alternans using the SV and PP controllers with B_a.

Calcium-driven Alternans with Control Applied Through the SR Calcium Load (B_l)

As shown in Table 9, for calcium-driven alternans, the best gains for the SV controller were only able to stabilize the unstable fixed points for periods of 190 ms or longer with the B_l control strategy. The PP controller performed better when compared with the SV controller for control applied through B_l, since all the maximum magnitudes of the closed loop eigenvalues were less than one; see Table 10.

Period (ms)	$\mathbf{K_{SV,B_l}}$	Max ($|\lambda_{SV,B_l}|$)
220	-0.78	0.9452
210	-1.10	0.9608
200	-1.30	0.9769
190	-1.44	0.9912
180	-1.54	1.0026
170	-1.61	1.0108

Table (9) Best gains for minimizing the closed-loop eigenvalue modulus for calcium-driven alternans using the SV controller with B_l.

Period (ms)	Max ($|\lambda_{SV,B_l}|$)	Max ($|\lambda_{PP,B_l}|$)
220	0.9452	0.9256
210	0.9608	0.9249
200	0.9769	0.9243
190	0.9912	0.9236
180	1.0026	0.9230
170	1.0108	0.9224

Table (10) Maximum closed-loop eigenvalue moduli for calcium-driven alternans using the SV and PP controllers with B_l.

III.4 Summary Comparison for State Feedback Controllers

One of our goals is to determine to what extent, if any, the controllability measures are predictive of the performance of different control strategies and algorithms; specifically, it would be helpful if larger controllability magnitudes corresponded to smaller gain values and smaller closed-loop eigenvalue moduli, since we could then use controllability analysis to predict the properties and impacts of specific control algorithms. We will consider in particular our more quantitative controllability measures, the minimum singular value magnitude of the controllability matrix and the cosine of the controllability angle. The latter quantity, $|\cos\theta_{ij}|$, is an indication of the difficulty of moving λ_i to a desired location in the complex plane via strategy B_j. Hence, we expect for the PP method that $\|K_{PP}\|$ should vary inversely with $|\cos\theta_{ij}|$, supposing that we chose $\|K_{PP}\|$ to move λ_i to a desired location and left all other eigenvalues in their original locations. However, $|\cos\theta_{ij}|$ may or may not vary inversely with SV or LQR gain values, since these algorithms may or may not have an impact on λ_i. Since the controllability matrix P is a mapping between the input sequence space and the state space, large $\sigma_{\min}(P)$ indicates that it is relatively easy to transfer the system from an initial state to a desired final state, but it is unclear how well $\sigma_{\min}(P)$ will align with specific gain magnitudes or closed-loop eigenvalue sizes.

For alternans due to voltage instability, the $\sigma_{\min}$ test predicted weak controllability through B_a and strong controllability through B_l. However, modal controllability ($|\cos\theta|$) predicted the reverse: strong controllability through B_a and weak controllability through B_l. Table 11 summarizes algorithms, control strategies, $|\cos\theta|$ of the maximum-modulus eigenvalue of the system (max $|\lambda_i|$), the gain value for the SV (K_{SV}) or norm of the gain vector ($\|K\|$) for the PP and LQR algorithms, and the maximum closed-loop eigenvalue modulus (max($|\lambda_{\mathrm{CL}}|$)). We only included results for the two control strategies that appeared to be the most promising based on the controllability results (B_a and B_l). Table 11 only covers one scenario, specifically a period of 240 ms, for the case of voltage-driven alternans. To aid in comparing control strategies, more favorable values (i.e., stronger controllability, smaller gains, or smaller closed loop eigenvalue moduli) are highlighted in blue.

Comparing the B_a and B_l control strategies, we observe from Table 11 that for the SV algorithm, larger $|\cos\theta|$ (i.e., stronger controllability of the maximum modulus eigenvalue) corresponds to smaller max($|\lambda_{\mathrm{CL}}|$), when $|K_{SV}|$ is held fixed at a value of 2.35. We were not able to find a positive

or negative K_{SV} that stabilized the fixed point for the B_l strategy, but $K_{SV} = 2.35$ is reported in the table, since it yielded a smaller $\max(|\lambda_{\mathrm{CL}}|)$ than $K_{SV} = -2.35$. In addition, we observe from Table 11 that for the PP algorithm, larger $|\cos\theta|$ corresponds to smaller $\|K_{PP}\|$, when comparing results from the two strategies B_a and B_l. Here, the largest eigenvalue was reassigned to 0.95, with all other eigenvalues left unchanged. Hence, the value $\max(|\lambda_{\mathrm{CL}}|) = 0.9505$ that appears in the table coincides with the magnitude of the second-largest open-loop eigenvalue. Furthermore, we observe from Table 11 that for the LQR algorithm, strategy B_a, which had a larger $|\cos\theta|$ value, yields both a smaller K_{LQR} and smaller $\max(|\lambda_{\mathrm{CL}}|)$ compared with B_l. Here, the R/Q ratio was fixed at 0.125 when computing the gains.

Algorithm	Strategy (B)	$\sigma_{\min}(P)$	$\lvert\cos\theta\rvert$ for $\max\lvert\lambda_i\rvert$	$K_{SV}, \|K_{PP}\|$ or $\|K_{LQR}\|$	$\max(\lvert\lambda_{\mathrm{CL}}\rvert)$
SV	B_a	2.63×10^{-5}	0.99	-2.35	0.84
	B_l	7.29×10^{-3}	0.09	2.35	1.56
PP	B_a	2.63×10^{-5}	0.99	2.48	0.9505
	B_l	7.29×10^{-3}	0.09	35.78	0.9505
LQR (R/Q = 0.125)	B_a	2.63×10^{-5}	0.99	1.36	0.84
	B_l	7.29×10^{-3}	0.09	8.73	0.86

Table (11) Controllers through the APD (*a*) and SR calcium (*l*) variables for voltage-driven alternans at a period of 240 ms.

In summary, for voltage-driven alternans at a period of 240 ms, all three controllers were consistent with $|\cos\theta|$ predictions (B_a is better) but not with $\sigma_{\min}$ predictions (B_l is better). The lack of consistency with $\sigma_{\min}$ may be a result of our choice to use gain size and $\max(|\lambda_{\mathrm{CL}}|)$ as indicators of control effort and performance, instead of other measures, such as the energy expended in transferring the initial state to a desired final state, which are more closely related to $\sigma_{\min}$ [45]. Moreover, SV was only successful through B_a, not B_l, since we were not able to find a stabilizing K_{SV} for B_l, regardless of the sign of K_{SV}. Non-zero controllability does not guarantee that SV control will work, since in general, all four elements of K may need to be nonzero to stabilize the fixed point. In addition, both PP and LQR control show smaller $\|K\|$ when $|\cos\theta|$ is larger, as expected.

For calcium-driven alternans, the $\sigma_{\min}$ test predicted that B_b, B_l, and B_a were all similarly good control strategies, where the the strategies are listed in decreasing order of the strength of controllability according to $\sigma_{\min}$. Modal controllability ($|\cos\theta|$) predicted strong controllability through either B_a or B_l but somewhat stronger through B_l. According to $|\cos\theta|$, the B_b strategy is helpful for controlling a stable eigenvalue that is the second-largest eigenvalue during alternans, but has less of an impact on the alternans eigenvalue. Table 12 shows related results for a period of 210 ms for the case of calcium-driven alternans. We observe that for the SV algorithm, when K_{SV} is fixed at -1.10, the larger $|\cos\theta|$ associated with B_l aligns with smaller $\max(|\lambda_{\mathrm{CL}}|)$, as expected, although the $\max(|\lambda_{\mathrm{CL}}|)$ values are similar for both strategies. In addition, for the PP algorithm, when $\max(|\lambda_{\mathrm{CL}}|)$ was held fixed at 0.95, larger $|\cos\theta|$ corresponded to smaller $\|K_{PP}\|$, which is consistent with our expectations. The LQR results did not show any obvious alignment with the modal controllability values, since a smaller $\max(|\lambda_{\mathrm{CL}}|)$ was achieved through applying the B_a strategy, whereas the B_l strategy yielded a smaller gain size.

Algorithm	Strategy (B)	$\sigma_{\min}(P)$	$\|\cos\theta\|$ for max $\|\lambda_i\|$	K_{SV}, $\|K_{PP}\|$ or $\|K_{LQR}\|$	$\max(\|\lambda_{\mathrm{CL}}\|)$
SV	B_a	4.24×10^{-3}	0.48	-1.10	0.97
	B_l	5.21×10^{-3}	0.86	-1.10	0.96
PP	B_a	4.24×10^{-3}	0.48	4.25	0.95
	B_l	5.21×10^{-3}	0.86	2.37	0.95
LQR (R/Q = 0.125)	B_a	4.24×10^{-3}	0.48	2.24	0.81
	B_l	5.21×10^{-3}	0.86	1.09	0.90

Table (12) Controllers through the APD (*a*) and SR calcium (*l*) variables for calcium-driven alternans at a period of 210 ms.

We found that the controllability measures we considered ($|\cos\theta|$ and $\sigma_{\min}$) both predicted that B_a and B_l are good strategies, though both favored B_l. In addition, SV and PP results were consistent with B_l being somewhat better (smaller $\max(|\lambda_{\mathrm{CL}}|)$ for SV and smaller $\|K\|$ for PP). LQR results were less straightforward to interpret, as holding R/Q fixed led to different combinations of $\max(|\lambda_{\mathrm{CL}}|)$ and $\|K\|$.

In summary, the modal controllability test gave a better prediction of control performance than the

minimum singular value test. This may be due to our choice of performance measures, $\max(|\lambda_{\text{CL}}|)$ and $\|K\|$. It is possible that a different criterion for performance, such as the 2-norm of the vector $[u_0, u_1, \ldots u_{n-1}]$ computed for a given control algorithm and a given choice of initial and final states, may show a relationship with $\sigma_{\min}$, since $\sigma_{\min}$ is inversely related to the theoretical minimum of this norm [45]. Comparing algorithms, we found that LQR and PP control algorithms were generally capable of stabilizing the fixed point, whereas SV control was not always capable of doing so. In comparing modal controllability results for different strategies, we find that the results in Tables 11 and 12 are consistent with those in Figs. 5 and 6 in the sense that all of them suggest that only the B_a strategy is a promising approach for suppressing both voltage- and calcium-driven alternans, at least for instabilities that are well captured by the two sets of model parameters we considered. For alternans driven only by calcium instability, the B_l strategy also may be viable, in addition to B_a.

Varying the R-Q ratio for Voltage and Calcium-Driven Alternans

Table 13 illustrates the impact of varying the R-Q ratios on the norm of the gain of the LQR controller ($\|K_{LQR}\|$) and the maximum closed-loop eigenvalue modulus ($\max(|\lambda_{LQR}|)$) for the voltage-driven alternans parameter set. We varied the R-Q ratios by starting with $\alpha_{RQ} = 2^0$ and repeatedly halving it until $\alpha_{RQ} = 2^{-9}$. When control was applied through a (i.e., $B = B_a$), $\|K_{LQR}\|$ increased and the $\max(|\lambda_{LQR}|)$ decreased as the R-Q ratio was progressively halved. This was the outcome we expected, since reducing α_{RQ} increases the penalty on the deviation of the state vector from the origin relative to the penalty on the control input, which should result in stronger feedback. When control was applied through l (i.e., $B = B_l$), both $\|K_{LQR}\|$ and $\max(|\lambda_{LQR}|)$ decreased as the R-Q ratio was halved. This trend for gain magnitudes is the opposite of what we expected, although we note that the changes in closed-loop eigenvalue moduli were relatively minor as α_{RQ} was varied, which may be due to weak controllability of the largest eigenvalue. For $\alpha_{RQ} \leq 2^{-2}$, both $\|K_{LQR}\|$ and $\max(|\lambda_{LQR}|)$ values were larger for B_l compared with B_a, which is consistent with the modal controllability result that B_a is a better strategy than B_l. For $\alpha_{RQ} = 2^0$ and 2^{-1}, relative to B_a, the B_l strategy yielded both larger $\|K_{LQR}\|$ but smaller $\max(|\lambda_{LQR}|)$, hence making it more challenging to make comparisons across strategies.

Table 14 shows how varying the R-Q ratio affects $\|K_{LQR}\|$ and $\max(|\lambda_{LQR}|)$ for calcium-driven alternans. When control was applied through a, $\|K_{LQR}\|$ increased and $\max(|\lambda_{LQR}|)$ decreased as the R-Q ratio was halved, which is the same trend that emerged in the voltage-driven case for the B_a strategy. When control was applied through l, $\|K_{LQR}\|$ increased and $\max(|\lambda_{LQR}|)$ decreased

Period (ms)	B	$\alpha_{RQ}\downarrow$	$\|(\mathbf{K_{LQR}})\|\uparrow$	$\max(|\lambda_{\mathbf{LQR}}|)\downarrow$	B	$\|(\mathbf{K_{LQR}})\|\downarrow$	$\max(|\lambda_{\mathbf{LQR}}|)\downarrow$
240	a	2^0	1.0871	0.90660	l	9.9450	0.86637
		2^{-1}	1.1854	0.88530		9.4252	0.86420
		2^{-2}	1.2817	0.86190		9.0124	0.86300
		2^{-3}	1.3602	0.84047		8.7296	0.86241
		2^{-4}	1.4145	0.82409		8.5578	0.86211
		2^{-5}	1.4475	0.81344		8.4619	0.86197
		2^{-6}	1.4659	0.80724		8.4111	0.86189
		2^{-7}	1.4758	0.80384		8.3845	0.86185
		2^{-8}	1.4808	0.80209		8.3711	0.86184
		2^{-9}	1.4834	0.80117		8.3643	0.86183

Table (13) Effect of the R-Q ratio α_{RQ} in the LQR controller for voltage-driven alternans (period = 240 ms).

Period (ms)	B	$\alpha_{RQ}\downarrow$	$\|(\mathbf{K_{LQR}})\|\uparrow$	$\max(|\lambda_{\mathbf{LQR}}|)\downarrow$	B	$\|(\mathbf{K_{LQR}})\|\uparrow$	$\max(|\lambda_{\mathbf{LQR}}|)\downarrow$
210	a	2^0	1.6489	0.87483	l	0.99411	0.90222
		2^{-1}	1.8977	0.85251		1.04320	0.89864
		2^{-2}	2.0971	0.83014		1.07160	0.89638
		2^{-3}	2.2353	0.81161		1.08700	0.89509
		2^{-4}	2.3200	0.79869		1.09500	0.89440
		2^{-5}	2.3676	0.79083		1.09910	0.89404
		2^{-6}	2.3929	0.78644		1.10120	0.89386
		2^{-7}	2.4062	0.78408		1.10220	0.89376
		2^{-8}	2.4128	0.78287		1.10280	0.89372
		2^{-9}	2.4162	0.78225		1.10300	0.89369

Table (14) Effect of the R-Q ratio α_{RQ} in the LQR controller for calcium-driven alternans (period = 210 ms).

as the R-Q ratio was halved, which also matches our predictions of the impact of decreasing α_{RQ}. The LQR gain norms for B_l were smaller than those for B_a, which is consistent with controllability results showing that B_l was a better strategy, although this is called into question somewhat by the lack of sensitivity of $\|K_{LQR}\|$ and $\max(|\lambda_{LQR}|)$ to changes in α_{RQ} for the B_l strategy.

III.4.1 LQR Closed-loop Eigenvalues and Linearized System Simulation Results

In this subsection we compare the magnitudes of the closed-loop eigenvalues across a range of periods for voltage- and calcium-driven alternans using two R-Q ratios (R = 2^{-9} $\|Q\|$ and R = 2^0 $\|Q\|$) We also show the behavior of x_k vs. iteration index (k) in response to LQR control for the linearized QSW model for selected alternans periods for the voltage-driven (240 ms) and calcium-driven (210 ms) alternans cases.

Closed-loop Eigenvalues and Simulation Results for Voltage-driven Alternans

Figure 7 shows the closed-loop eigenvalue magnitudes for the voltage-driven alternans case. The eigenvalues were generally closer to the origin when $R = 2^{-9}$ $\|Q\|$ compared to when $R = 2^0$ $\|Q\|$. This finding fits with our expectation that reducing the R-Q ratio should lead to smaller max($|\lambda_{LQR}|$), which was also shown in Table 13. Based on the B_a and B_l results in Fig. 7, it is not entirely clear which strategy yields the more favorable closed-loop eigenvalue placements, although the B_a strategy appears to avoid the peak in magnitude that occurs for one of the two larger eigenvalues near $T = 300$ ms.

Figure 8 shows the evolution of the deviational state vector x_k for the voltage-driven alternans case at a period of 240 ms. The plots were obtained from a simulation of the closed-loop linearized system $x_{k+1} = (A - BK_{LQR})x_k$ for initial condition $x_0 = \begin{bmatrix} 0.1 & 0.1 & 0.1 & 0.1 \end{bmatrix}^T$ We observe that x_k converged to zero when control was applied through either a or l. As expected, the convergence was faster for the smaller R-Q ratio $\alpha_{RQ} = 2^{-9}$ compared to $\alpha_{RQ} = 2^0$.

(a) $\alpha_{RQ} = 2^0 \, \|Q\|$

(b) $\alpha_{RQ} = 2^{-9} \|Q\|_2$

(c) $\alpha_{RQ} = 2^0 \, \|Q\|$
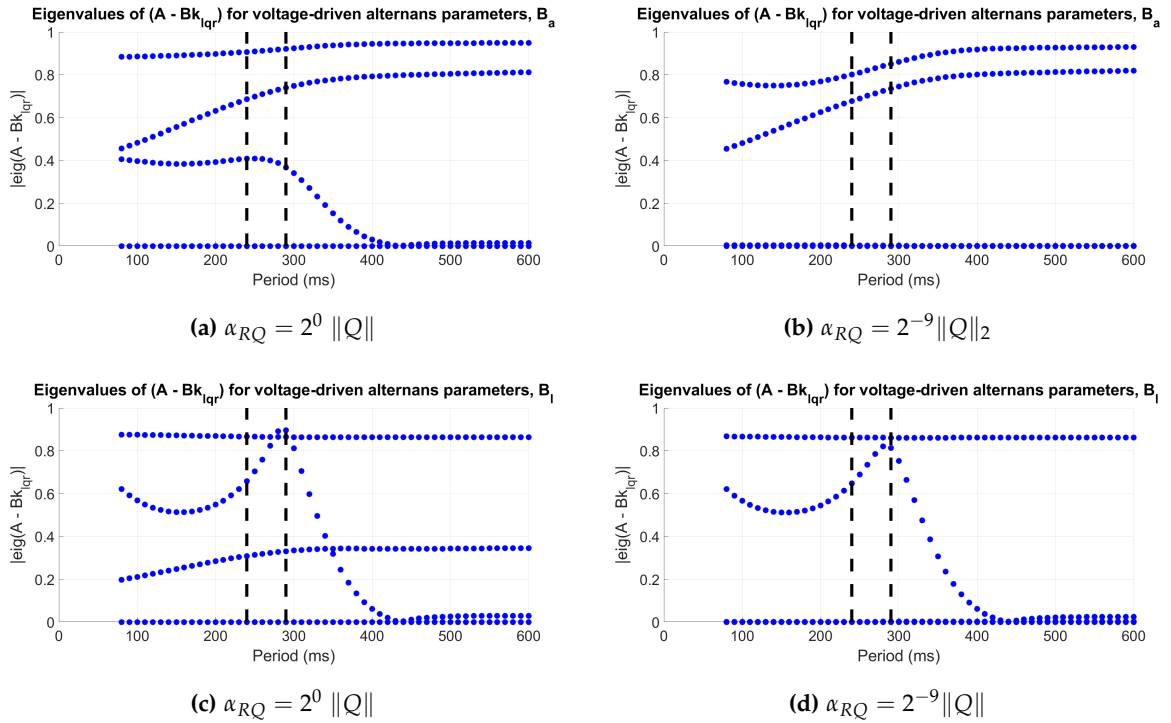
(d) $\alpha_{RQ} = 2^{-9} \|Q\|$

Figure (7) Closed-loop eigenvalues for voltage-driven alternans in the QSW model for two different control strategies and for two different R-Q ratios. (a) B_a and $\alpha_{RQ} = 2^0$. (b) B_a and $\alpha_{RQ} = 2^{-9}$. (c) B_l and $\alpha_{RQ} = 2^0$. (d) B_l and $\alpha_{RQ} = 2^{-9}$. The periods within the dashed vertical lines are the periods that are in the alternans regime and whose APD values are less than the period (thereby avoiding 2:1 block).

(a) $\alpha_{RQ} = 2^0 \, \|Q\|$

(b) $\alpha_{RQ} = 2^{-9}\|Q\|$

(c) $\alpha_{RQ} = 2^0 \, \|Q\|$
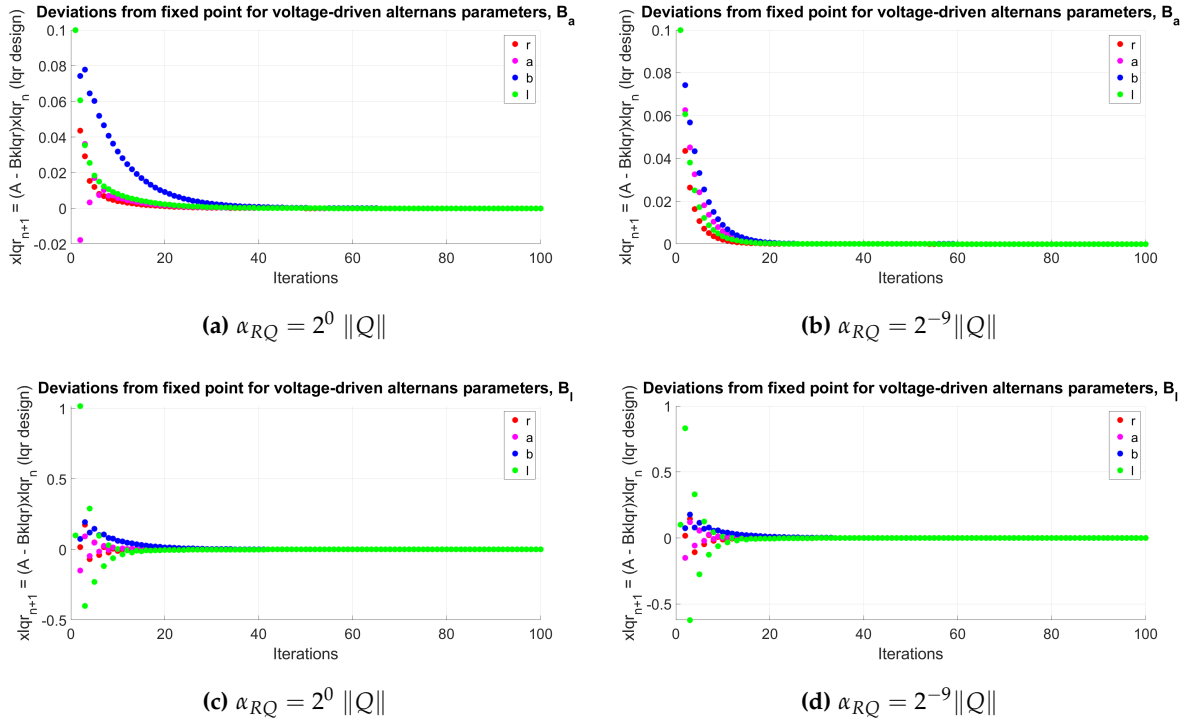
(d) $\alpha_{RQ} = 2^{-9}\|Q\|$

Figure (8) Deviational state vector components of the linearized system for voltage-driven alternans using two control strategies and two values of α_{RQ}. (a) B_a and $\alpha_{RQ} = 2^0$. (b) B_a and $\alpha_{RQ} = 2^{-9}$. (c) B_l and $\alpha_{RQ} = 2^0$ (d) B_l and $\alpha_{RQ} = 2^{-9}$.

Closed-loop Eigenvalues and Simulation Results for Calcium-driven Alternans

We next consider the closed-loop eigenvalues for calcium-driven alternans. Figure 9 shows closed-loop eigenvalue magnitudes as a function of period. The eigenvalues, on average, appear to be closer to the origin for $\alpha_{RQ} = 2^{-9}$ compared to $\alpha_{RQ} = 2^0$, which is consistent with our findings in Table 14. However, comparing Figs. 9 (c) and (d) confirms that the larger closed-loop eigenvalues are mostly insensitive to changes in α_{RQ}, which was also seen in Table 14. It is difficult to determine whether the figure supports the controllability prediction that B_l is better than B_a for reassigning the alternans eigenvalue. The larger closed-loop eigenvalues appear to be closer to the origin under B_a in Fig. 9, but Table 14 indicates that larger gains were obtained for the B_a strategy.

(a) $\alpha_{RQ} = 2^0 \, \|Q\|$

(b) $\alpha_{RQ} = 2^{-9} \|Q\|$

(c) $\alpha_{RQ} = 2^0 \, \|Q\|$
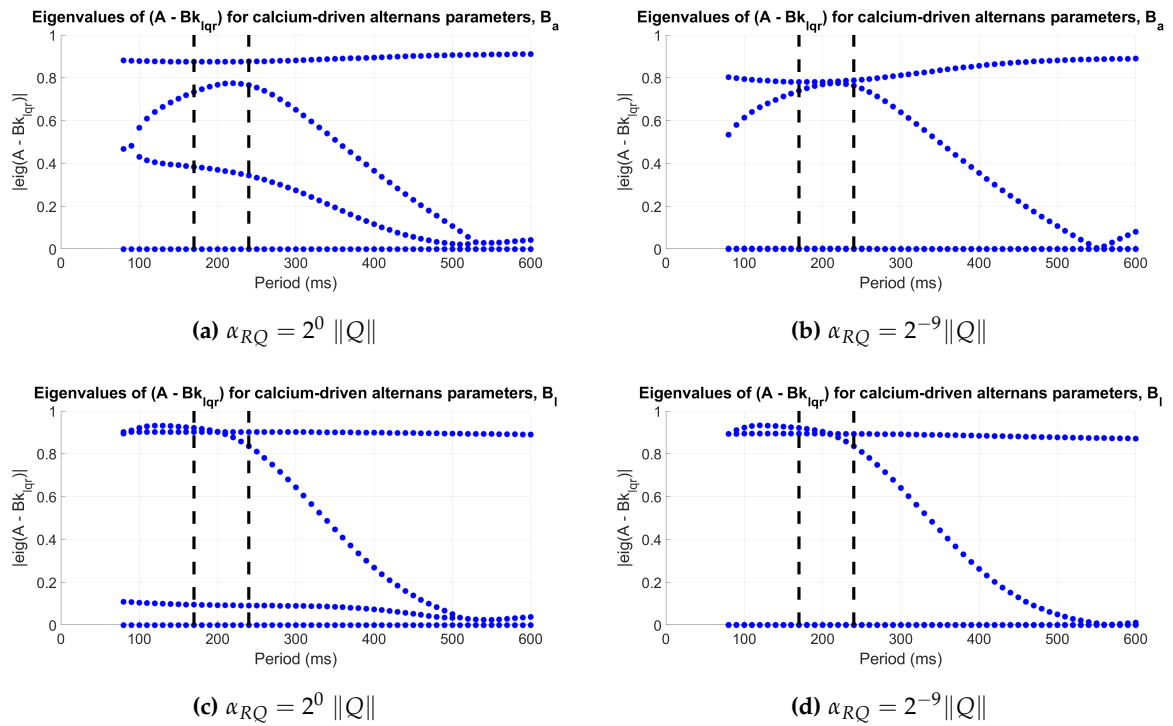
(d) $\alpha_{RQ} = 2^{-9} \|Q\|$

Figure (9) Closed-loop eigenvalues for calcium-driven alternans in the QSW model for two different control strategies and for two different R-Q ratios. (a) B_a and $\alpha_{RQ} = 2^0$. (b) B_a and $\alpha_{RQ} = 2^{-9}$. (c) B_l and $\alpha_{RQ} = 2^0$. (d) B_l and $\alpha_{RQ} = 2^{-9}$. The periods within the dashed vertical lines are the periods that are in the alternans regime and whose APD values are less than the period (thereby avoiding 2:1 block).

Figure 10 shows x_k vs. k for calcium-driven alternans at a period of 210 ms. The deviations converged to zero when control was applied through either a or l, as expected. The deviations converged faster when control was applied through a compared to l, but this is difficult to use as a means to compare strategies, given that we showed that holding α_{RQ} fixed does not necessarily lead to equal gain sizes. We also observed that convergence was faster for the smaller R-Q ratio ($\alpha_{RQ} = 2^{-9}$ compared to $\alpha_{RQ} = 2^0$).

(a) $\alpha_{RQ} = 2^0 \, \|Q\|$

(b) $\alpha_{RQ} = 2^{-9} \|Q\|$

(c) $\alpha_{RQ} = 2^0 \, \|Q\|$
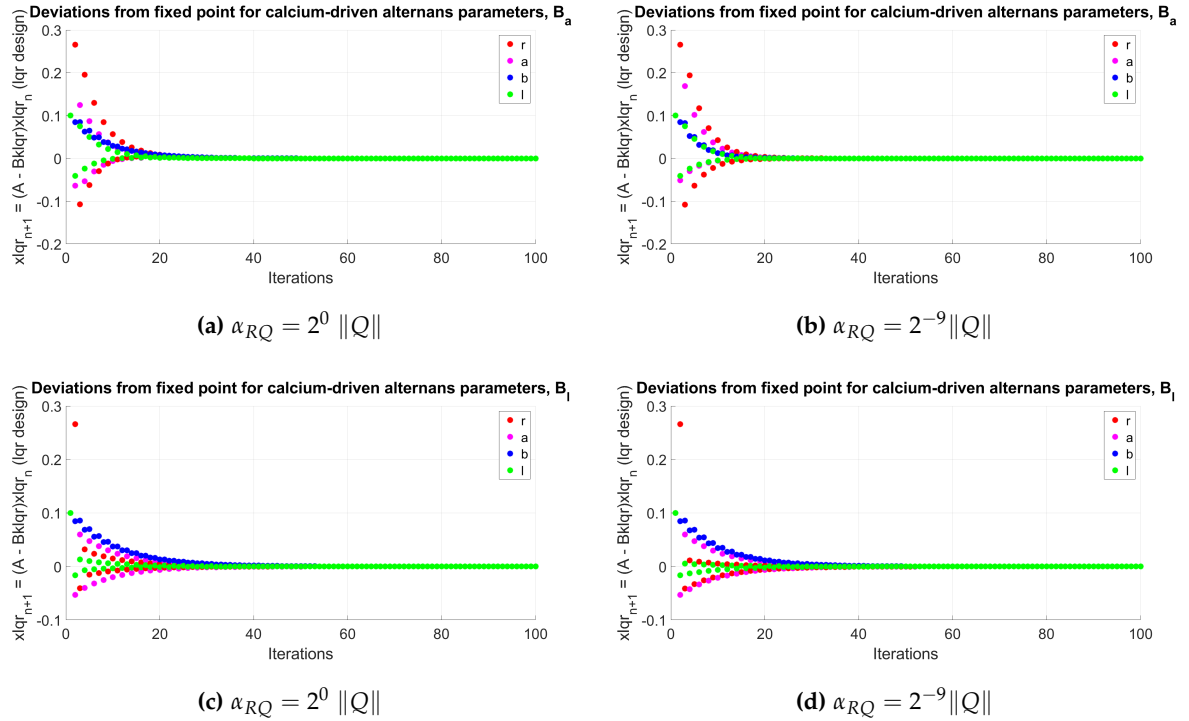
(d) $\alpha_{RQ} = 2^{-9} \|Q\|$

Figure (10)   Deviational state vector components of the linearized system for calcium-driven alternans using two control strategies and two values of α_{RQ}. (a) B_a and $\alpha_{RQ} = 2^0$. (b) B_a and $\alpha_{RQ} = 2^{-9}$. (c) B_l and $\alpha_{RQ} = 2^0$ (d) B_l and $\alpha_{RQ} = 2^{-9}$.

III.5   Eigenvalue Analysis of the SSK Model

As part of this thesis, we began an analysis of the SSK model and successfully completed several of the first steps needed for assessing controllability. A full analysis of controllability and the effectiveness of different control algorithms for stabilizing unstable fixed points for this system is reserved for future work.

III.5.1   Fixed Points

The first step we needed to complete was calculation of the fixed points of the beat-to-beat map of the SSK model. We computed the fixed points as described in the Methods section. Fixed points were readily found for both voltage- and calcium-driven alternans when the maximum number of nonlinear iterations (`maxit`), the maximum number of inner iterations (`maxitl`), and the tolerance (`tol`) in the Newton-Krylov solver were set to 90, 90, and 10^{-12} respectively. The maximum iteration values had to be increased beyond the default value of 40 in order to find fixed point estimates that met the tolerance.

III.5.2   Selection of the Step Size Used in Numerical Approximation of the Jacobians

To assess stability of the fixed points, it is necessary to analyze the Jacobian of the linearized SSK beat-to-beat map evaluated at each fixed point. Because of the absence of an analytical form for the map, the Jacobian must be evaluated using a numerical approach. We used a finite-difference approximation, which necessitated choosing a step size for evaluating the partial derivatives. We evaluated the impact of the step size used in the numerical approximation of the Jacobians, as described in the Methods section, by calculating the norm of the difference in Jacobian eigenvalues corresponding to neighboring step sizes, where the step size was varied over negative integer powers of 10. We sought to identify a step size that would cause the smallest possible changes in the Jacobian eigenvalues if that step size were changed slightly.

The range of step sizes for which the eigenvalues were changing the least was found to be approximately 10^{-3} to 10^{-6} for both voltage- and calcium-driven alternans. Figure 11 shows the norms of the differences with respect to the Jacobian step sizes. For voltage-driven alternans, the minimum of the norm of the differences occurs for step sizes in the range of 10^{-4} to 10^{-6}. For calcium-driven alternans, the interval of least change is somewhat longer, covering a range of approximately 10^{-3} to 10^{-6}. For simplicity, we prefer to have a common Jacobian step size for both parameter sets; thus, we chose a step size of 10^{-5} for both cases.

III.5.3   Eigenvalues

Using the Jacobian step size obtained as described above, we calculated the moduli of the eigenvalues of the Jacobian evaluated at the fixed point as a function of period for both voltage- and calcium-driven alternans, as illustrated in Fig. 12. (Recall that Fig. 1(c)(d) shows the values

(a) Voltage-driven alternans

(b) Calcium-driven alternans
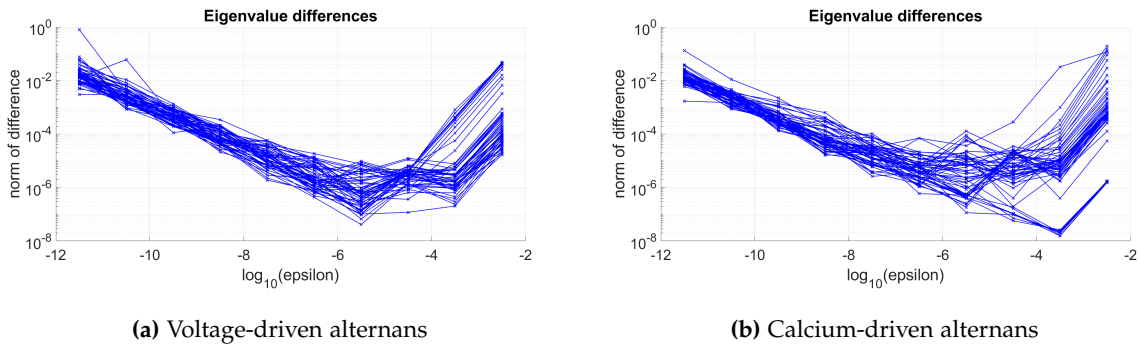
Figure (11)   Norms of the differences in the eigenvalues of the linearized beat-to-beat map for neighboring values of the step size for (a) voltage- and (b) calcium-driven alternans as the step size ϵ is varied. Each individual curve corresponds to the norms of the eigenvalue differences for a single period, as a function of step size.

of one variable at the fixed point across a range of cycle lengths for both alternans scenarios.) Figure 12a shows that for voltage-driven alternans, the fixed point loses stability at a period of about 370 ms when the maximum eigenvalue modulus exceeds one. Similarly, for calcium-driven alternans, the fixed point becomes unstable at a period of about 450 ms, as shown in Fig. 12b.

(a)

(b)
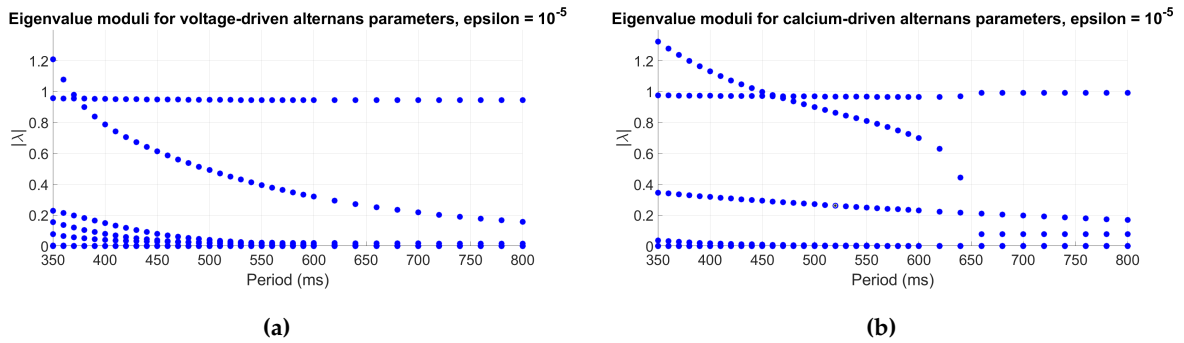
Figure (12)   Moduli of the eigenvalues of the linearized beat-to-beat map for (a) voltage- and (b) calcium-driven alternans using a step size of 10^{-5}.

IV. Discussion and Conclusion

Understanding the effectiveness of control strategies for cardiac alternans, including the variables through which they work more effectively and the impact of alternans mechanism (voltage or calcium) could be useful in preventing life-threatening arrhythmias such as ventricular fibrillation. In this thesis we first studied the controllability of the QSW model using three different measures of controllability and then compared the controllability results against a measure of control effort (the norm of the feedback gain) for selected cases. Our first test, the controllability matrix rank test, indicated that the system was not controllable through the calcium release variable but was controllable through all other variables, regardless of alternans mechanism. Our second method, which was based on the minimum singular values of controllability matrices, showed strong and weak controllability through the SR load and APD, respectively, for voltage-driven alternans and strong controllability through the SR load, APD, and total Ca concentration for calcium-driven alternans. Our last test, the modal controllability test, indicated strong and weak controllability through APD and SR Ca load, respectively, for voltage-driven alternans and strong controllability through the APD or SR load for calcium-driven alternans (but somewhat stronger for the latter).

In addition, we designed three controllers for the QSW model to test our controllability findings: the single-variable (SV), pole placement (PP), and Linear Quadratic Regulator (LQR) controllers. For voltage-driven alternans, we found, for a selected period, that applying control through APD was successful in stabilizing the unstable fixed point, and thus eliminating alternans, for each of the controllers. The SV controller could not achieve stabilization through the SR calcium load, but both the PP and LQR controllers could do so, although not as easily (higher gain required) as through APD. These two controllers also showed a smaller gain matrix magnitude (easier to control) for larger controllability angle cosine magnitude (more controllable), as expected. All three controllers performed consistently with the modal controllability test that favored controlling through APD and disagreed with the prediction from the minimum singular value test that favored controlling through SR calcium load. For many of our control algorithm tests, regardless of the alternans mechanisms, we only tried controlling through the APD or SR load variables, since those appeared to be among the more promising strategies according to our controllability tests. Control through other variables was not explored as thoroughly. For alternans driven by instabilities in intracellular calcium, we found for a selected period that all three controllers could stabilize the unstable fixed point when control was applied through either the APD or SR calcium

load. Control was shown to be roughly equally easy through APD and SR calcium load for the SV controller and easier through SR calcium load for PP (smaller gain); for the LQR controller, a smaller maximum eigenvalue could be achieved by controlling through APD, but control through SR calcium load required a smaller gain. The SV and PP controllers performed consistently with predictions from the modal controllability test that control could be achieved more easily through SR Ca load than through APD, although none of the findings were inconsistent with the minimum singular value test results, which predicted strong controllability through SR Ca load as well as APD, as control could be achieved in all cases through either variable. For the LQR controller, the question of which variable was better for use in control algorithms depended on whether greater priority was given to achieving a smaller eigenvalue or a smaller gain value.

Overall, for the QSW model with voltage-driven alternans induced by steepening the APD restitution curve and calcium-driven alternans induced by increasing the strength of SR uptake, our analysis showed that control of alternans could be accomplished more easily through the APD variable for voltage-driven alternans and through the SR calcium load variable for calcium-driven alternans. We found that the rank test provided the least information and that the modal controllability test generally gave more accurate predictions of control algorithm performance than the minimum singular value test. This may be due to our choice of performance measures. The minimum singular value test gives information about the control strategy that minimizes the energy expended in controlling the system [45], and control energy is different from the measures (maximum closed-loop eigenvalue modulus and gain size) that we used to evaluate the performance of the control algorithms. Among the controllers, the SV approach was the least effective at stabilizing the fixed points. Note that direct comparison of the PP and LQR methods is not straightforward, especially given the performance measures we have chosen, since it is difficult to hold either the maximum closed-loop eigenvalue modulus or the gain size fixed across algorithms. In the case of PP, the gain is computed based on the choice of closed-loop eigenvalues, while for LQR, both the gain and eigenvalues are consequences of the choice of Q and R.

Our results are consistent with a well-known result from control theory, which is that mutli-variable state feedback should generally be able to outperform single-variable feedback, since multi-variable feedback gives us more degrees of freedom through which we can manipulate the closed-loop eigenvalues. That is, single-variable feedback, which corresponds to a $1 \times n$ gain vector (K) with only one nonzero entry, will not be able to impact as many elements of the closed-loop Jacobian ($A - BK$) compared with multi-variable feedback, where all entries of K are typically nonzero. The downside of multi-variable feedback is that it usually requires all of the state

variables to be measured or estimated. If some of the state variables cannot be measured directly, a standard approach is to design an observer or Kalman filter that reconstructs unmeasured state variables from available data. Among multi-variable algorithms, LQR is often preferred over PP, since LQR has favorable properties, such as a degree of robustness to modeling errors [46], which PP is not guaranteed to have. However, PP control is easier to compare with modal controllability predictions.

We also looked briefly at the SSK model. For this model, controllability is more complicated to assess, both because it involves significantly more state variables (16) and because it is a continuous-time model, thus necessitating the definition of a discrete-time beat-to-beat map. Although it was beyond the scope of the present work to perform a full controllability analysis for the SSK model, we completed some of the most difficult initial steps, including computing fixed points, Jacobian matrices, and eigenvalues of the Jacobian for the discrete map in different parameter regimes. We note that we are not the first to perform a linear stability analysis on a myocyte model with realistic internal calcium dynamics. Related work includes Li and Otani's linearization and controllability analysis of the Fox-McHarg-Gilmour myocyte model [18], an examination of alternans mechanisms in SSK and other models [47], studies of subcellular alternans [35, 48, 49], and investigations of empirical data-based estimation of SSK eigenvalues [50, 51]. However, as stated previously, these studies either did not compare different alternans mechanisms [18] or did not include any investigation of controllability properties [35, 47, 48, 50, 49, 51].

IV.1   Limitations

Our study includes several important limitations. We investigated controllability only for the QSW model, and those results provided a basis for implementing state feedback controllers for the linearized system. We do not know how applicable our results are to other models or to the heart more broadly. In particular, our findings concerning the best ways to control voltage- and calcium-driven alternans may be limited by the model we chose or the specific ways in which these alternans mechanisms are implemented in the model; in particular, other models may produce calcium alternans through different mechanisms. More generally, we do not know whether alternans in the heart is driven primarily by voltage or calcium, by a combination of the two, or perhaps by other mechanisms.

Furthermore, our results showed that control strategies through the SR load were useful for eliminating calcium-driven alternans. However, beat-to-beat perturbation of any calcium concentration

currently is not technologically feasible. Applying control strategies to the APD is the most feasible experimentally, since APD can be adjusted by applying an electrical current to the tissue. In addition, our work is somewhat limited by the hand-tuning of the gain and desired eigenvalues when implementing the SV and the PP controllers, respectively. It may be possible that better choices exist (associated with lower gain, for example) that were not considered as part of the hand-tuning process. Another limitation of our work is that our controllability and algorithm tests were confined to linearized models; although our results are valid for sufficiently small excursions from fixed points, our findings may not be accurate for larger deviations.

IV.2   Future Work

Many directions of the research presented here could lead to interesting future work. We could test controllability using a combination of two or more variables of the QSW model. For example, applying a proportional feedback current through calcium ion channels would affect both the APD a and the total calcium b. In the present work, we confined our analysis to a small number of controllability measures (rank, $\sigma_{\min}$, and modal) for the sake of tractability, but we could consider other measures of controllability, such as the condition number of the controllability matrix P. In addition, we only designed feedback controllers for the linearized QSW model. A more realistic result could be obtained by implementing the controllers on the nonlinear system. Furthermore, we could compare our findings with the results of other types of control schemes that do not rely on state feedback, such as constant diastolic interval pacing [8, 37], to determine whether our controllability analysis makes helpful predictions in such contexts.

Another planned step is to apply a nondimensionalizing transformation to the linearized QSW model. Reference values for each of the variables remain to be determined, but nondimensionalizing the model will aid us in making fairer comparisons across control strategies, given that some of the state variables have different units. We will also extend the comparisons made between controllability measures and performance measures (such as feedback gain size) to cover a wider range of alternans periods.

It is worth noting that our minimum singular value controllability tests did not always favor the same control strategies as the modal controllability tests. One possible explanation is that the discrepancies are due to different state variables having different units, hence nondimensionalizing the linearized QSW system could resolve these disagreements. Another possible explanation is based on the fact that the controllability measures, while related to one another, capture different

aspects of the ease with which a system may be controlled. The modal controllability measure indicates how easy or difficult it is to use a specific control strategy to move a specific eigenvalue. In contrast, the minimum singular value of the controllability matrix is related to the "control energy" needed to move the system from one point in the state space to another. The control "energy," which is really just the 2-norm of the vector containing the sequence of control inputs, is usually defined as $E = \sum_{k=0}^{k_f - 1} \|u_k\|^2$. The minimum singular value of the controllability matrix is inversely related to the theoretical minimum of E, where the minimum is taken over all possible input sequences from $k = 0$ to $k = k_f - 1$ [45]. If we were to compute E for each of the control algorithms we tested, along with the theoretical minimum of E, these should show a better correspondence with the minimum singular value measures, compared with the modal measures. Of the three control algorithms we investigated, LQR most closely resembles a minimum energy control strategy, due to the "energy-like" $u_k^T R u_k$ term in the cost function, so it is not entirely clear why the minimum singular value measure was not always inversely related to the LQR gain sizes. After nondimensionalizing the QSW model, we aim to determine whether there is a relationship between $\sigma_{\min}$ values belonging to different B_j strategies and the corresponding LQR control energies for some range of R-Q ratios. For example, when $R = 1$ and Q approaches zero, the LQR cost more closely resembles E, so we would expect to see a relationship between gains and $\sigma_{\min}$.

We also would like to apply our controllability analysis to other models that support both voltage- and calcium-driven alternans, including both discrete-time and continuous-time models (such as the SSK model), to determine the generality of our findings. Furthermore, we could extend our analysis from the case of a single cell to spatially extended systems with one, two, or three spatial dimensions. Finally, our work may be useful in providing insights leading to the design of novel control strategies.

References

[1] G. A. Roth, C. Johnson, A. Abajobir, F. Abd-Allah *et al.*, "Global, regional, and national burden of cardiovascular diseases for 10 causes, 1990 to 2015," *Journal of the American College of Cardiology*, vol. 70, no. 1, pp. 1–25, Jul. 2017.

[2] E. J. Benjamin, P. Muntner, A. Alonso, M. S. Bittencourt *et al.*, "Heart disease and stroke statistics—2019 update: A report from the American Heart Association," *Circulation*, vol. 139, no. 10, Mar. 2019.

[3] D. J. Christini, M. L. Riccio, C. A. Culianu, J. J. Fox *et al.*, "Control of electrical alternans in canine cardiac Purkinje fibers," *Physical Review Letters*, vol. 96, no. 10, p. 104101, 2006.

[4] M. R. Guevara, G. Ward, A. Shrier, and L. Glass, "Electrical alternans and period doubling bifurcations," *Computers in Cardiology*, vol. 562, pp. 167–170, 1984.

[5] G. M. Hall and D. J. Gauthier, "Experimental control of cardiac muscle alternans," *Physical Review Letters*, vol. 88, no. 19, p. 198102, 2002.

[6] G. R. Mines, "On dynamic equilibrium in the heart," *The Journal of Physiology*, vol. 46, no. 4-5, pp. 349–383, 1913.

[7] K. Hall, D. J. Christini, M. Tremblay, J. J. Collins *et al.*, "Dynamic control of cardiac alternans," *Physical Review Letters*, vol. 78, no. 23, p. 4518, 1997.

[8] R. Wu and A. Patwardhan, "Mechanism of repolarization alternans has restitution of action potential duration dependent and independent components," *Journal of Cardiovascular Electrophysiology*, vol. 17, no. 1, pp. 87–93, Jan. 2006.

[9] E. Ott, C. Grebogi, and J. A. Yorke, "Controlling chaos," *Physical Review Letters*, vol. 64, no. 11, pp. 1196–1199, Mar. 1990.

[10] K. Pyragas, "Continuous control of chaos by self-controlling feedback," *Physics Letters A*, vol. 170, no. 6, pp. 421–428, Nov. 1992.

[11] D. J. Christini, K. M. Stein, S. M. Markowitz, S. Mittal *et al.*, "Nonlinear-dynamical arrhythmia control in humans," *Proceedings of the National Academy of Sciences*, vol. 98, no. 10, pp. 5827–5832, May 2001.

[12] W. L. Ditto, M. L. Spano, V. In, J. Neff *et al.*, "Control of human atrial fibrillation," *International Journal of Bifurcation and Chaos*, vol. 10, no. 03, pp. 593–601, Mar. 2000.

[13] B. Echebarria and A. Karma, "Spatiotemporal control of cardiac alternans," *Chaos: An Interdisciplinary Journal of Nonlinear Science*, vol. 12, no. 3, pp. 923–930, 2002.

[14] A. Garfinkel, M. Spano, W. Ditto, and J. Weiss, "Controlling cardiac chaos," *Science*, vol. 257, no. 5074, pp. 1230–1235, Aug. 1992.

[15] L. M. Muñoz, J. F. Stockton, and N. F. Otani, "Applications of control theory to the dynamics and propagation of cardiac action potentials," *Annals of Biomedical Engineering*, vol. 38, no. 9, pp. 2865–2876, 2010.

[16] A. Garzón, R. O. Grigoriev, and F. H. Fenton, "Model-based control of cardiac alternans in Purkinje fibers," *Physical Review E*, vol. 84, no. 4, p. 041927, 2011.

[17] A. Garzón, R. O. Grigoriev, and F. H. Fenton, "Continuous-time control of alternans in long Purkinje fibers," *Chaos: An Interdisciplinary Journal of Nonlinear Science*, vol. 24, no. 3, p. 033124, Sep. 2014.

[18] M. Li and N. F. Otani, "Controlling alternans in cardiac cells," *Annals of Biomedical Engineering*, vol. 32, no. 6, pp. 784–792, 2004.

[19] S. Dubljevic, S. F. Lin, and P. D. Christofides, "Studies on feedback control of cardiac alternans," *Computers & Chemical Engineering*, vol. 32, no. 9, pp. 2086–2098, 2008.

[20] C. D. Marcotte and R. O. Grigoriev, "Adjoint eigenfunctions of temporally recurrent single-spiral solutions in a simple model of atrial fibrillation," *Chaos: An Interdisciplinary Journal of Nonlinear Science*, vol. 26, no. 9, p. 093107, Sep. 2016.

[21] S. Aniţa and V. Barbu, "Local exact controllability of a reaction-diffusion system," *Differential and Integral Equations*, vol. 14, no. 5, pp. 577–587, 2001.

[22] G. Wang and L. Zhang, "Exact Local Controllability of a One-Control Reaction-Diffusion System," *Journal of Optimization Theory and Applications*, vol. 131, no. 3, pp. 453–467, Dec. 2006.

[23] M. Bendahmane and F. W. Chaves-Silva, "Null controllability of a degenerated reaction–diffusion system in cardiac electro-physiology," *Comptes Rendus Mathematique*, vol. 350, no. 11-12, pp. 587–590, Jun. 2012.

[24] F. W. Chaves-Silva and M. Bendahmane, "Uniform Null Controllability for a Degenerating Reaction-Diffusion System Approximating a Simplified Cardiac Model," *SIAM Journal on Control and Optimization*, vol. 53, no. 6, pp. 3483–3502, Jan. 2015.

[25] T. Breiten and K. Kunisch, "Compensator design for the monodomain equations with the FitzHughNagumo model," *ESAIM: Control, Optimisation and Calculus of Variations*, vol. 23, no. 1, pp. 241–262, Jan. 2017.

[26] J. B. Nolasco and R. W. Dahlen, "A graphic method for the study of alternation in cardiac action potentials," *Journal of Applied Physiology*, vol. 25, no. 2, pp. 191–196, Aug. 1968.

[27] E. Chudin, J. Goldhaber, A. Garfinkel, J. Weiss *et al.*, "Intracellular Ca(2+) dynamics and the stability of ventricular tachycardia," *Biophysical Journal*, vol. 77, no. 6, pp. 2930–2941, Dec. 1999.

[28] D. A. Eisner, H. S. Choi, M. E. Diaz, S. C. O'Neill *et al.*, "Integrative analysis of calcium cycling in cardiac muscle," *Circulation Research*, vol. 87, no. 12, pp. 1087–1094, 2000.

[29] Y. Shiferaw, M. A. Watanabe, A. Garfinkel, J. N. Weiss *et al.*, "Model of intracellular calcium cycling in ventricular myocytes," *Biophysical Journal*, vol. 85, no. 6, pp. 3666–3686, Dec. 2003.

[30] T. O'Hara, L. Virág, A. Varró, and Y. Rudy, "Simulation of the undiseased human cardiac ventricular action potential: Model formulation and experimental validation," *PLoS Comput Biol*, vol. 7, no. 5, p. e1002061, May 2011.

[31] Z. Qu, Y. Shiferaw, and J. N. Weiss, "Nonlinear dynamics of cardiac excitation-contraction coupling: an iterated map study," *Physical Review. E, Statistical, Nonlinear, and Soft Matter Physics*, vol. 75, no. 1 Pt 1, p. 011927, Jan. 2007.

[32] Y. Shiferaw, D. Sato, and A. Karma, "Coupled dynamics of voltage and calcium in paced cardiac cells," *Physical Review E*, vol. 71, no. 2, p. 021903, 2005.

[33] S. H. Weinberg, "Impaired sarcoplasmic reticulum calcium uptake and release promote electromechanically and spatially discordant alternans: A computational study," *Clinical Medicine Insights: Cardiology*, vol. 10, pp. CMC–S39 709, 2016.

[34] J. J. Fox, J. L. McHarg, and R. F. Gilmour Jr, "Ionic mechanism of electrical alternans," *American Journal of Physiology-Heart and Circulatory Physiology*, vol. 282, no. 2, pp. H516–H530, 2002.

[35] W. Groenendaal, F. A. Ortega, T. Krogh-Madsen, and D. J. Christini, "Voltage and calcium dynamics both underlie cellular alternans in cardiac myocytes," *Biophysical Journal*, vol. 106, no. 10, pp. 2222–2232, May 2014.

[36] S. Rush and H. Larsen, "A practical algorithm for solving dynamic membrane equations," *IEEE Transactions on Bio-Medical Engineering*, vol. 25, no. 4, pp. 389–392, Jul. 1978.

[37] E. M. Cherry, "Distinguishing mechanisms for alternans in cardiac cells using constant-diastolic-interval pacing," *Chaos: An Interdisciplinary Journal of Nonlinear Science*, vol. 27, no. 9, p. 093902, Aug. 2017.

[38] W. L. Brogan, *Modern Control Theory (3rd ed.)*.   Upper Saddle River, NJ, USA: Prentice-Hall, Inc, 1991.

[39] C. T. Kelley, *Solving Nonlinear Equations with Newton's Method*, ser. Fundamentals of Algorithms. Philadelphia: SIAM, 2003, no. 1.

[40] D. A. Knoll and D. E. Keyes, "Jacobian-free Newton-Krylov methods: a survey of approaches and applications," *Journal of Computational Physics*, vol. 193, no. 2, pp. 357–397, 2004.

[41] T. Kailath, *Linear Systems*, ser. Prentice-Hall information and system science series.   Englewood Cliffs, N.J: Prentice-Hall, 1980.

[42] Guofeng Yao and Xuefei Gao, "Controllability of regular systems and defective systems with repeated eigenvalues," *Journal of Vibration and Control*, vol. 17, no. 10, pp. 1574–1581, Sep. 2011.

[43] A. M. A. Hamdan and A. H. Nayfeh, "Measures of modal controllability and observability for first-and second-order linear systems," *Journal of Guidance, Control, and Dynamics*, vol. 12, no. 3, pp. 421–428, 1989.

[44] H. Kwakernaak and R. Sivan, *Linear Optimal Control Systems*.   New York: Wiley Interscience, 1972.

[45] A. E. Bryson and Y.-C. Ho, *Applied Optimal Control: Optimization, Estimation, and Control*, rev. print ed.   New York: Taylor & Francis, 1975.

[46] U. Shaked, "Guaranteed stability margins for the discrete-time linear quadratic optimal regulator," *IEEE Transactions on Automatic Control*, vol. 31, no. 2, pp. 162–165, Feb. 1986.

[47] P. N. Jordan and D. J. Christini, "Characterizing the contribution of voltage- and calcium-dependent coupling to action potential stability: implications for repolarization alternans," *American Journal of Physiology-Heart and Circulatory Physiology*, vol. 293, no. 4, pp. H2109–H2118, Oct. 2007.

[48] S. A. Gaeta, T. Krogh-Madsen, and D. J. Christini, "Feedback-control induced pattern formation in cardiac myocytes: A mathematical modeling study," *Journal of Theoretical Biology*, vol. 266, no. 3, pp. 408–418, Oct. 2010.

[49] Y. Shiferaw and A. Karma, "Turing instability mediated by voltage and calcium diffusion in paced cardiac cells," *Proceedings of the National Academy of Sciences*, vol. 103, no. 15, pp. 5670–5675, Apr. 2006.

[50] A. Petrie and X. Zhao, "Estimating eigenvalues of dynamical systems from time series with applications to predicting cardiac alternans," *Proceedings of the Royal Society A: Mathematical, Physical and Engineering Sciences*, vol. 468, no. 2147, pp. 3649–3666, Nov. 2012.

[51] X. Zhao, D. G. Schaeffer, W. Krassowska, and D. J. Gauthier, "A model-independent technique for eigenvalue identification and its application in predicting cardiac alternans," in *Volume 2: Biomedical and Biotechnology Engineering*.   Seattle, Washington, USA: ASME, 2007, pp. 301–302.